THE EFFECT OF ABRASIVE WATER JET TURNING PARAMETER OF INCONEL 718 ALLOY DIMENSIONAL ACCURACY AND SURFACE ROUGHNESS

This report is submitted in accordance with requirement of the Universiti Teknikal Malaysia Melaka (UTeM) for Bachelor Degree of Manufacturing Engineering (Hons.)

by

AINAA SHAMIRA BINTI JEFRI

FACULTY OF MANUFACTURING ENGINEERING

2021

DECLARATION

I hereby, declared this report entitled "The Effect of Abrasive Water Jet Turning Parameter of Inconel 718 Alloy Dimensional Accuracy and Surface Roughness" is the result of my own research except as cited in references.

Signature   : ....
Author's Name   : AINAA SHAMIRA BINTI JEFRI
Date   : 08 February 2021

APPROVAL

This report is submitted to the Faculty of Manufacturing Engineering of Universiti Teknikal Malaysia Melaka as a partial fulfilment of the requirement for Degree of Manufacturing Engineering (Hons). The member of the supervisory committee is as follow:

....

(PM DR. MOHD SHAHIR BIN KASIM)

ABSTRAK

Mesin konvensional mempunyai banyak masalah, terutamanya dari segi jangka hayat alat, produktiviti, dan kemasan permukaan. Abrasive Water Jet Turning (AWJT) adalah alternatif untuk pemesinan konvensional. AWJT adalah sejenis proses pemesinan yang tidak konvensional yang menggunakan jet air bertekanan tinggi yang dicampurkan bersama-sama dengan zarah kasar. Ia sangat sesuai untuk bahan yang paling sukar dan bahan kerja silinder. Inconel 718 Alloy adalah bahan yang akan digunakan untuk projek ini. Aloi Inconel 718 dikenali sebagai bahan paling sukar dan sangat sukar untuk mesin menggunakan kaedah konvensional. Inconel 718 Alloy mempunyai kombinasi ketahanan kakisan, ketahanan pengoksidaan dan ketahanan merayap yang sangat baik. Bahan jenis ini biasanya terdapat di industri kapal terbang.

Penyediaan bahan, menjalankan mesin, pengumpulan data, dan analisis data adalah empat tahap dalam penyelesaian projek ini. 8 sampel dengan diameter 16 mm dan panjang 50 mm akan dimesin menggunakan mesin AWJT. Reka bentuk full factorial terlibat dalam projek ini untuk memastikan bahawa eksperimen dijalankan secara sistematik dan cekap. Semua data dikumpulkan dengan menggunakan mesin kekasaran permukaan dan mesin penguji kebulatan. Data dianalisis dengan mengunakan ANOVA dan untuk mengenal pasti kesan signifikan parameter dioptimumkan atau tidak.

ABSTRACT

Conventional machines have a lot of problems, particularly in terms of tool life, productivity, and surface finishing. Abrasive Water Jet Turn (AWJT) is an alternative to conventional machining. AWJT is a type of unconventional machining process that uses a high-pressure water jet that is mixed together with abrasive particles. It is very suitable for the hardest material and cylindrical workpieces. Inconel 718 Alloy is the material that will be used for this project. Inconel 718 alloy is known as the hardest material and is very difficult to machine using conventional methods. Inconel 718 Alloy has an excellent combination of corrosion resistance, oxidation resistance and creep resistance. This type of material is usually found in the aircraft industry.

The preparation, experimentation, data collection, and data analysis are four stages in the completion of this project. 8 samples with a diameter of 16 mm and a length of 50 mm will be machined using the AWJT machine. A full factorial design is involved in this project to ensure that the experiment is carried out in a systematic and efficient manner. All the data is collected by using a surface roughness machine and a roundness tester machine. The data is analyzed by using ANOVA and to identify the significant effect of the parameter is optimized or not.

DEDICATION

To my beloved father, Jefri bin Muhamad,

my appreciated mother, Norliza binti Yaacob,

my adored sister and brother, Efi, Emy and Ernie,

for giving me moral support, money, cooperation, encouragement, and also understandings

Thank You So Much & Love You All Forever

My Supervisor,

PM Dr. Mohd Shahir bin Kasim,

for guiding me through the whole research project

My friends and technician especially Mr. Syafiq,

The Water Jet lab technician who is involved in this study and project,

May Allah ease our journey and bless all of us. InshaAllah.

ACKNOWLEDGMENT

By The Name of Allah the Most Merciful and Gracious

My highest gratitude and praise to Allah S.W.T for the blessing that I can finish my final year project. Through this subject, I learned a lot of experience in the engineering field. First of all, thanks to my lovely parents for giving encouragement, enthusiasm, and invaluable assistance to me. Without all this, I might not be able to complete his final year project properly. Second, I would like to express my deepest appreciation to all those who provided me the possibility to complete this report. A special gratitude I give to my supervisor PM Dr. Shahir bin Kasim for her advice, guidance, constant supervision as well as exposing me to meaningful experiences throughout the study. I am truly grateful for his unwavering support throughout the whole period of this final year project. Taught all the manufacturing knowledge, share the experience with me, and taught me how to generate an excellent format report.

Furthermore, I would also like to acknowledge with much appreciation the crucial role of the staff of the Faculty of Manufacturing Engineering (FKP) and Faculty of Mechanical and Manufacturing Engineering Technology (FTKMP), who permitted to use all required equipment and the necessary materials to complete the study. Last but not least, I want to thank all lecturers, staff, and my friends who had to help me going through this study and for all knowledge and experiences that I have gained which lead to the completion of my study.

TABLE OF CONTENTS

LIST OF TABLES

LIST OF FIGURES

LIST OF ABBREVIATIONS, SYMBOLS, AND NOMENCLATURES

AWJ	-	Abrasive Water Jet
AWJT	-	Abrasive Water Jet Turning
AWJM	-	Abrasive Water Jet Milling
NNS	-	Net Near Shape
3D	-	Three dimension
MRR		Material Removal Rate
SEM	-	Scanning Electron Microscope
DoE	-	Design of Experiment
DOC	-	Depth Of Cut
CNC	-	Computer Numerical Control
CCD	-	Central Composite Design
CAD	-	Computer-Aided Design
CAM	-	Computer-Aided Manufacturing
ANOVA	-	Analysis of Variance
DF	-	Degree of Freedom
SS	-	Sum of Square
MS	-	Mean Square
LLL	-	Life Long Learning
DTI	-	Dial Tester Indicator

R	-	Roundness
f	-	Feed rate
N	-	Rotational Speed
Ra	-	Surface Roughness
Dim_e	-	Diameter Error
A	-	Area
p	-	Perimeter
e	-	Eccentricity
b	-	Minor axis
a	-	Major axis
%	-	Percent
mm	-	Millimetre
µm	-	Micrometer
°C	-	Degree Celsius
MPa	-	Mega Pascal
mm/min	-	Millimetre per minute
m/min	-	Meter per minute
cm/min	-	Centimeter per minute
rpm	-	Revolution per minute
Hz	-	Hertz
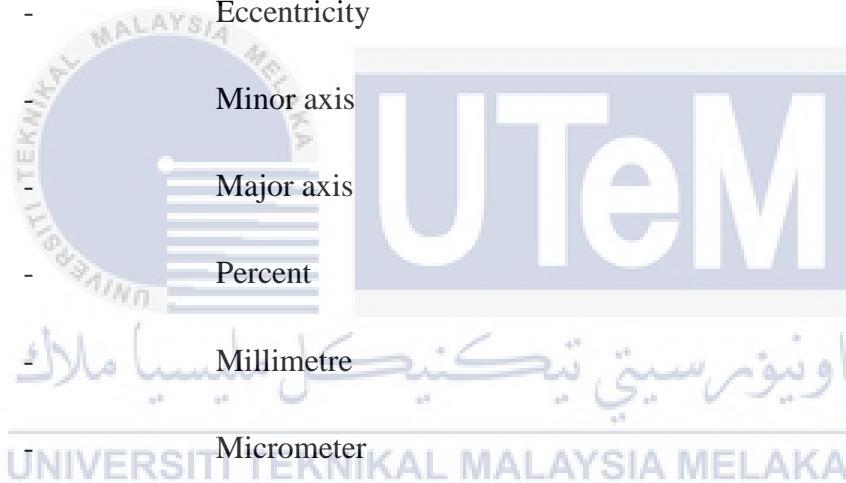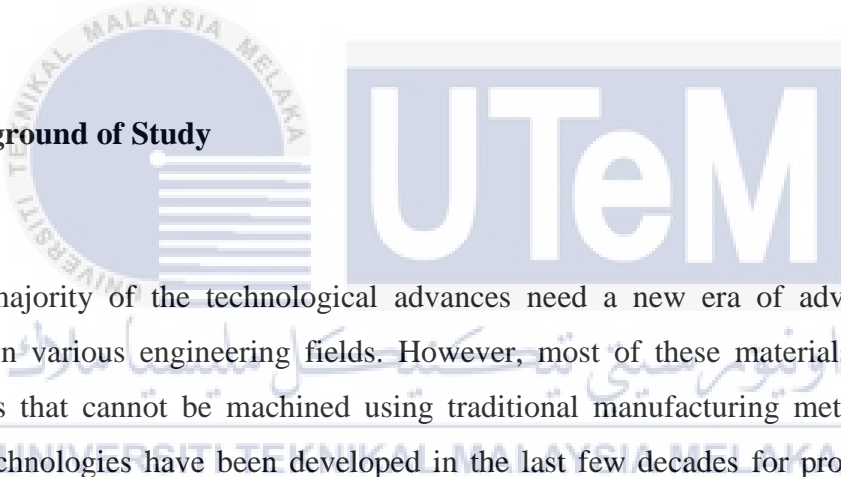
| g/s | - | Gram per second |
| mm/s | - | Milimeter per second |

CHAPTER 1

INTRODUCTION

1.1 Background of Study

The majority of the technological advances need a new era of advanced material applications in various engineering fields. However, most of these materials have specific characteristics that cannot be machined using traditional manufacturing methods. Different machining technologies have been developed in the last few decades for processing several shapes of components.

Unfortunately, each of these technologies has its limitations for giving excellent efficiency and accuracy. Meanwhile, Abrasive Water Jet (AWJ) machining has been proven to cut various material shapes without any excessive force or thermal damage. AWJ machining often finds work cutting hardened steels, Ti- alloys, aerospace alloys, and other materials that are difficult to machine using conventional methods.

Water jet technology is one of the fastest-growing major machine tool processes globally because of its flexibility and simple operation. The garnet abrasive is used in the water jet stream. Without the abrasive, it can cut soft material only. Abrasive water jet can cut any thickness from smallest to most significant in high or low volume. There are two types of

AWJ machining: Abrasive Water Jet Turning (AWJT) and Abrasive Water Jet Milling (AWJM).

AWJT is usually used to reduce the diameter of a cylindrical workpiece. The main difference between AWJT and AWJM is that the part that will be machined will rotate for turning operation, while for milling operation, the tools will rotate. AWJT is a technology that uses a high-pressure water jet that combines with abrasive particles. This technology is very suitable for the most challenging material that is very difficult to remove the unwanted shape. AWJT technology is also ideal for turning near net shape (NNS) and profiling grinding wheels.

In this research, AWJT will be discussed due to their ability to machine more rigid material such as Inconel 718 alloy with a cylindrical shape. Inconel 718 alloy is usually used on aircraft turbine engines for the aerospace industry. The modern aircraft turbine engines offer more reliability than the existing aircraft turbine engines. The most important factors to react to the higher reliability for the turbine engines are that the engineering teams must ensure these engines can be maintained, used for several years, and have excellent efficiency.

Inconel 718 alloy, also known as super alloys where the material can be machined at a temperature exceeding 1300˚F. It is also one of the materials that are very difficult to machine. In the aircraft industry, the Inconel 718 alloy is the perfect material to withstand various higher temperature corrosions and stress conditions that can occur in the turbine engine. Inconel 718 alloy also has an excellent combination of high-temperature corrosion resistance, oxidation resistance, and creep resistance. During machining Inconel 718 alloys, there will be several challenges such as generates more heat at the tooltip, causing excessive tool wear, and others. The other application for Inconel 718 alloy is 3D printing technology, die casting, oil and gas industries, saltwater applications, and others.

1.2   Problem Statement

Inconel 718 Alloy's material has become one of the commonly used in the aerospace industry, chemical industry, and others. Nowadays, this material has been frequently used in gas turbine engines because Inconel 718 alloy has excellent tensile strength, ductility, fracture toughness, creep resistance, and fatigue resistance. Vrushali and Dalu (2017) states that it is difficult to machine the Inconel 718 Alloy material by using a conventional method due to Inconel 718 alloy produces poor results during the machining process Inconel 718 alloy tends to react with cutting tool material at the highest temperature.

Conventional machining has been used widely in the field of metal processing. When it comes to machining the material, the most important of traditional machining is physical contact between the tool and the workpiece. Thus, it can lead to tool wear since physical contact is required to perform the work. Friction is one factor of tool wear where the amount of heat is generated during the machining process. Anthony *et al.*(2017) conducted a study about the tool wear during machining Inconel 718 alloy concluded that in machining the Inconel 718 alloy material, the tool wear is influenced by thermal softening, adhesion, diffusion, notching, and thermal cracking. Thus, it can conclude that several factors were influenced during machining Inconel 718 alloy using conventional machining.

During the metal cutting using the conventional method, the metal will absorb the heat that transmits away from the cutting, and it will cause the heat-affected zone on the workpiece. It occurs when the material of the workpiece, which is Inconel 718 alloy, is harder than the tool's material. Heat affected zone is also known as a non-melted area of metal and directly affects the surface roughness of the workpiece.

Abrasive Water Jet Turning (AWJT) is the best solution to overcome these problems. Unfortunately, the study of surface roughness of the Inconel 718 alloy and productivity is questionable. The research about the parameter of AWJT is very important to overcome all the problem occurs in conventional lathe machine and to increase the knowledge of the appropriate parameter to produce the highest quality of the product by using AWJT.

1.3   Objectives

The objectives of the report are:

a) To investigate the relationship between cutting parameter on surface roughness and dimensional accuracy.

b) To suggest a prediction model for surface roughness and dimensional accuracy by using full factorial design.

c) To propose and validate the best combination parameter to optimized the responses.

1.4   Scope Of Research

The scope of research for this project is the evaluation of the surface characteristic of Inconel 718 alloy. The effect of machining parameters on the surface characteristic and the value of roundness and eccentricity measurement during machining Inconel 718 alloy of 16 mm diameter and 50 mm length in size using abrasive water jet turning (AWJT) processes is the main focus for this research. This project was carried out by experimenting on eight samples of Inconel 718 alloy material. The material of abrasive used for the AWJT machine is garnet mesh size 80.

CHAPTER 2

LITERATURE REVIEW

2.1 Abrasive Water Jet

Abrasive water jet machining (AJM) is a mechanical material removal process used to erode and cavities by the effect of the slurry abrasive particles on hard and fragile materials. Since the procedure is non-thermal, non-chemical, and non-electrical, there is no change in the work piece's metallurgical and physical properties. AJM can cut and mill several materials without excessive force or thermal damage, and AJM does not involve any hazardous material or equipment (Nouhi *et al.*,2015). Ushasta *et al.* (2014) also noted that by using AWJ, there is no thermal distortion, flexibility, versatility, minimum absence of heat-affected zone, and others.

Machining of abrasive water jet generally involves a water pumping system, abrasive feeding system, abrasive jet nozzle, and catcher (Jain and V.K., 2002). Ushasta *et al.* (2014) point out some important mechanisms about the AWJ where pumping system delivers water at high speeds by the increasing pressure of water specified mass flow rate and requires a high power motor connected to the intensifier with high intensifier ratio.

2.2   Inconel 718 Alloy Material

Inconel 718 alloy is an alloy that operates at a high fraction of melting point. Inconel 718 alloy also develops resistance to high-temperature strength by solid solution strengthening. According to Thakur *et al.* (2009) and Ravindra and Sharad (2012), Inconel 718 material is commonly used in aircraft engine parts, pressure vessels, turbine power plants, and the automotive sector due to their unique characteristics such as low thermal conductivity, hardness, hardening, an affinity for reacting with tool material, high shear strength and others. According to Amato *et al.*'s (2012) research by using the Selective Laser Melting (SLM) process, they found that Inconel 718 has good mechanical properties (up to 700˚C) and suitable for a critical component in turbine engines.

2.3   Abrasive Water Jet Turning Parameter

2.3.1   The effect of depth of cut

The next important parameter in order to determine the higher quality of the material is the depth of cut (DOC). Liu *et al.* (2014) explored the depth of cut for alumina ceramics by using Abrasive Water Jet Turning (AWJT) is influenced by the traverse speed and followed by tilt angle, abrasive flow rate, and pressure. They also found that the maximum DOC is obtained when the factor of pressure and tilt angle is equal to 320 MPa and 90˚, respectively. With the interactive effect, the effect on DOC was not significant. The optimal state of the cycle would result in a higher DOC of 480 µm according to the first criterion while the maximum DOC of 390 µm for the second criterion.
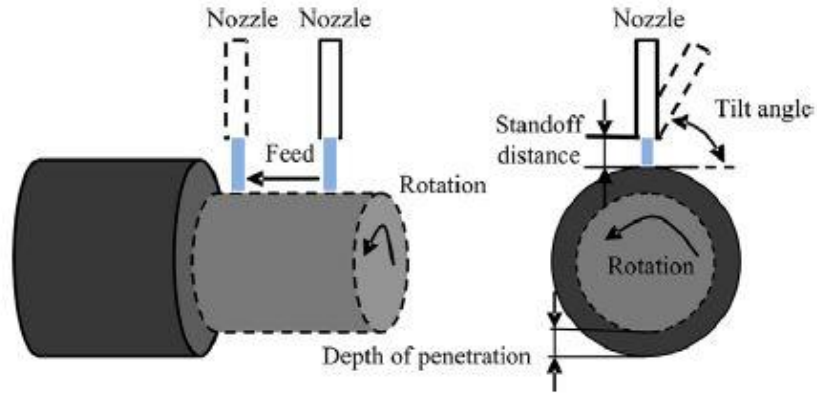
Figure 2.1: Schematic diagram of AWJT radial-mode turning (Liu *et al.*,2014)

Srivastava *et al.* (2017) conducted a study about the surface integrity in the tangential turning of hybrid MMC A359/B4C/AL2O3 by abrasive water jet. They concluded that the maximum value for compressive residual stresses is 275 MPa, 265 MPa, and 215 MPa at 50 µm for the measurement of the depth from the surface of the machine sample at 10, 20, and 30 mm/min, respectively of traverse speed (Figure 2.2). Arola D and Ramulu M also concluded the same range of residual stress of AWJ machined surface.
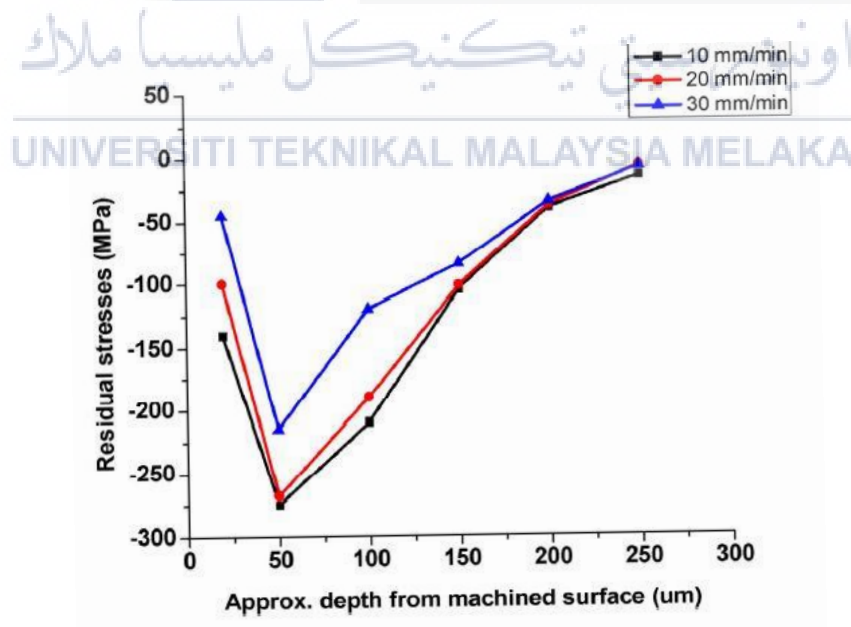
Figure 2.2: Residual stresses Vs depth from the machined surface (Srivastava *et al.*,2017)

7

Srivastava *et al.*(2017) further studied the microhardness against the depth from the machined surface. They found that the maximum value of microhardness is 217 HV, 211 HV, and 208 HV for 50 μm for the measurement of the depth from the surface machined sampled at 10, 20, 30 mm/min of traverse speed. They also observed the variation of microhardness from the initial sample's value before turning operation is in the range of 7% to 9%. Akkurt (2009) also states the same observation about the variation of microhardness. Srivastava *et al.*(2017) concluded that the depth value increases towards the core of the sample. The value of microhardness is almost equal to the microhardness of the sample manufactured before machining. Table 2.1 shows the compilation depth of the cut parameter of AWJT from the literature.
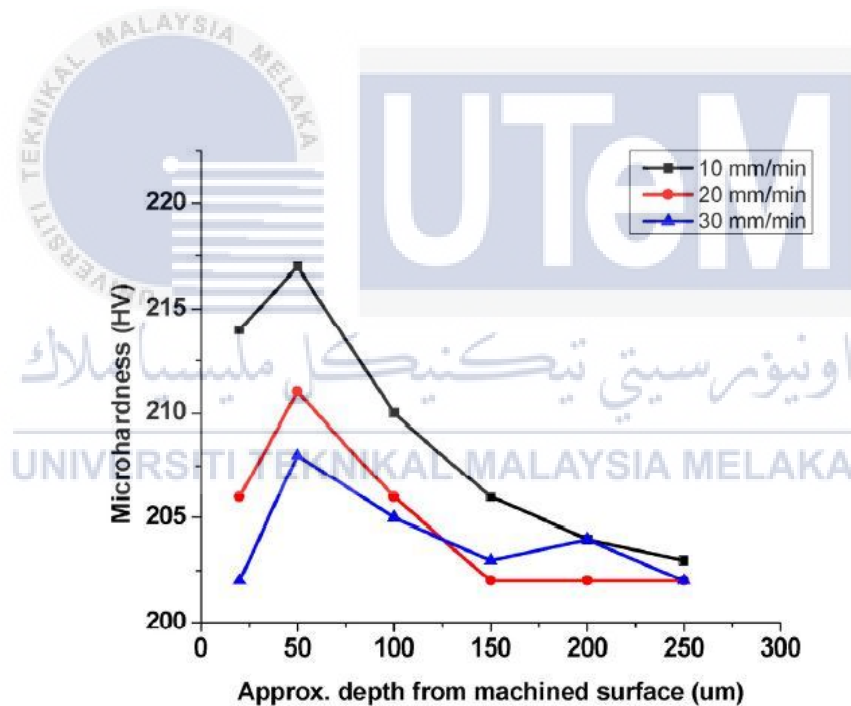
Figure 2.3: Microhardness Vs depth from machined surface (Srivastava *et al.*,2017)

Table 2.1: The compilation depth of cut parameter of AWJT from literature

Author	Parameters/ Methods	Findings/ Observations
Niranjan C.A *et al.* (2018)	Water pressure = 100 - 300 MPa	The value of DOC increased when the value of water pressure increased.
	Traverse speed = 300-500 mm/min	DOC is lower when the traverse speed is high.
	Two-way ANOVA	Water pressure parameters were the significant parameters affecting DOC in this study, followed by traverse speed Water pressure = 85.94% Traverse speed = 11.66%
J. Wang (2008)	Abrasive flow rate = 1.6, 9.8, 12.1, 14.4 g/s	When the value of DOC increases when the value abrasive flow rate increase.
	Traverse speed = 0.167, 0.333, 0.5, 0.667 mm/s	The value of DOC decreased when the value traverse speed increased.
	Water pressure = 275, 310, 345, 380 MPa	The value of DOC increased when the value of water pressure increased.
Liu *et al.* (2014)	Standoff distance = 2, 6 , 10 mm	The value of DOC increased when the value stand-off distance increased.
	Tilt angle = 60˚, 75˚, 90˚	The value of DOC decreased when the value tilt angle increased. The maximum DOC can be obtained when the tilt angle is equal to 90˚
	Water pressure = 200, 260, 320 MPa	The value of DOC increased when the value of water pressure increased. The maximum DOC can be obtained when the water pressure is equal to 320 MPa
	Traverse speed = 0.1, 0.3, 0.5 mm/s	The value of DOC decreased when the value traverse speed increased.

2.3.2 The effect of rotational speed

Figure 2.4 shows that the spindle speed influences the average surface roughness during AWJT of the Inconel 718 alloy. Fuat *et al.* (2016) found that when the constant amount of abrasives impacting the different points on the workpieces, it will generate a lower speed that is enough to remove material depending on the material properties. They reported that the spindle speed was had a bigger impact on the surface roughness, where the average surface roughness was improved by 55% when the spindle speed increased from 25min^{-1} to 100min^{-1}.

9

Based on N. Satheesh Kumar *et al.*(2012)'s experiment on five different types of Carbon steel material by using a CNC turning machine, they observed that the value of surface roughness in the unit of µm decreased when the rotational speed of the spindle is increased. Table 2.2 showing the compilation rotational speed parameter of AWJT from literature.
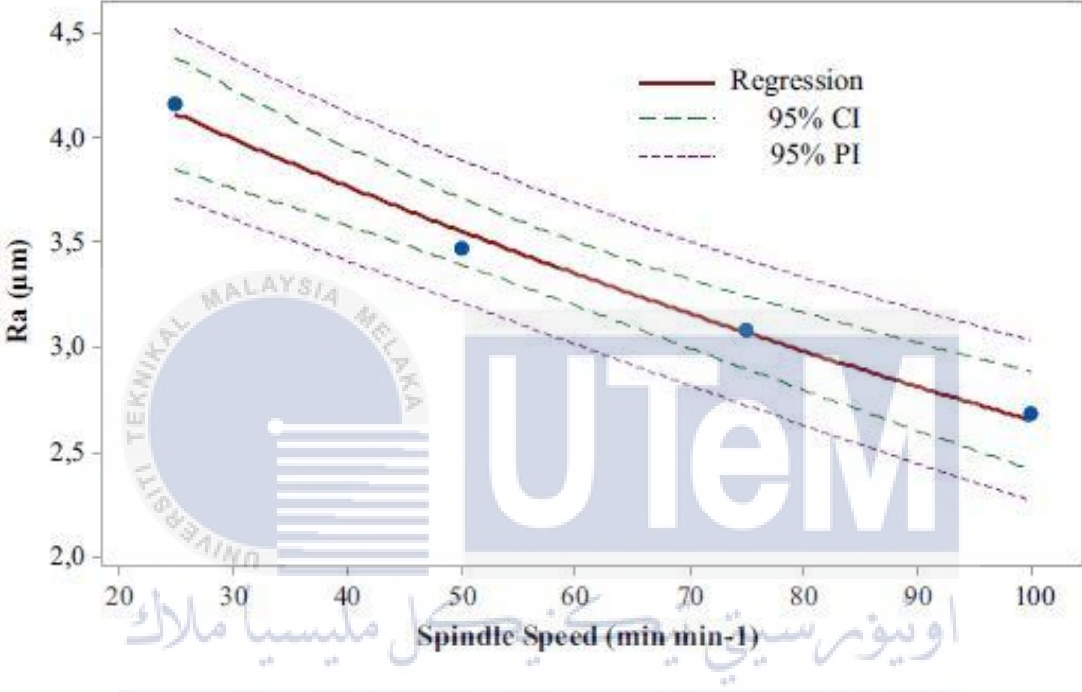
Figure 2.4: Effect of spindle speed on the surface roughness (Fuat *et al.* (2016)

Table 2.2: The compilation rotational speed parameter of AWJT from literature.

Author	Parameters/ Methods	Findings/ Observations
Fuat *et al.*(2016)	Rotational speed = 25, 50, 75, 100 m/min	55% of average surface roughness improved when the spindle speed increased from 25 m/min to 100 m/min.
N. Satheesh Kumar *et al.*(2012)	Rotational speed = 339-980 rpm	Surface roughness decreased when the rotational speed is increased.
D. M. Addona *et al.* (2017)	Rotational speed = 60, 90, 190, 255 m/min	The low speed of the spindle produces the same results of surface roughness for a longer period
		The value of surface roughness is high when the rotational speed at lower speeds
Weiyi Li *et al.* (2013)	Rotational speed = 0.3, 0.6, 1.2, 2.4 m/s	The rotational speed is influenced by the DOC
		DOC increase by 14% when the rotational speed increased to 0.3 m/s to 2.4 m/s
		The value of surface roughness when the rotational speed decreased.

2.3.3 The effect of feed rate/ traverse speed

Fuat *et al.* (2016) revealed that the feed rate of the nozzle had a connection to the amount of Abrasive Water Jet (AWJ) that had an impact on the workpieces. Based on the following figures, the value of surface roughness is increased by 16% when the feed rate of the nozzle increased from 10 mm/min to 25 mm/min.

11
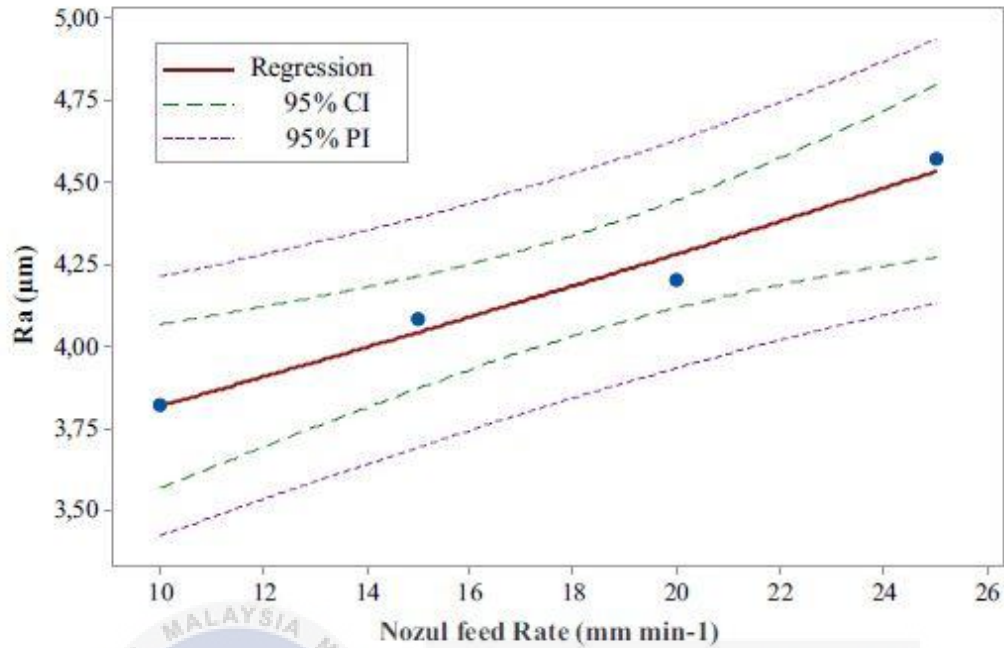
Figure 2.5: Surface Roughness in μm Vs Nozzle Feed Rate in mm/min (Fuat *et al.*, 2016)

The traverse speed is related to the percentage of reduction in diameter and averages MRR (Srivastava *et al.*, 2017). Figure 2.6 shows that there are decreased trends that occur in the percentage of reduction in diameter when the traverse speed is increased from 10mm/min to 30 mm/min. Phenomena occur as the interaction time of the abrasive particle with the machining surface decreases as the traversing speed increases, resulting in a decrease in the number of impacts. Besides, Figure 2.7 shows the traverse speed influenced by MRR. Based on Figure 2.7, the average value of MRR decreased by 13.81% when the traverse speed increased at 30 mm/min. Table 2.3 showing the compilation feed rate parameter of AWJT from the literature.
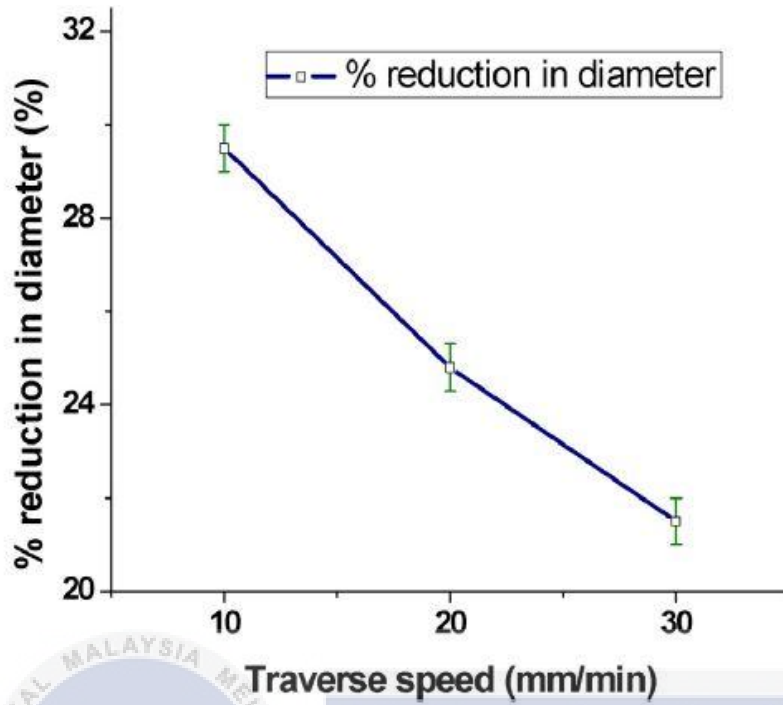
Figure 2.6: Percentage of reduction in diameter Vs Traverse Speed (Srivastava *et al.*, 2017).
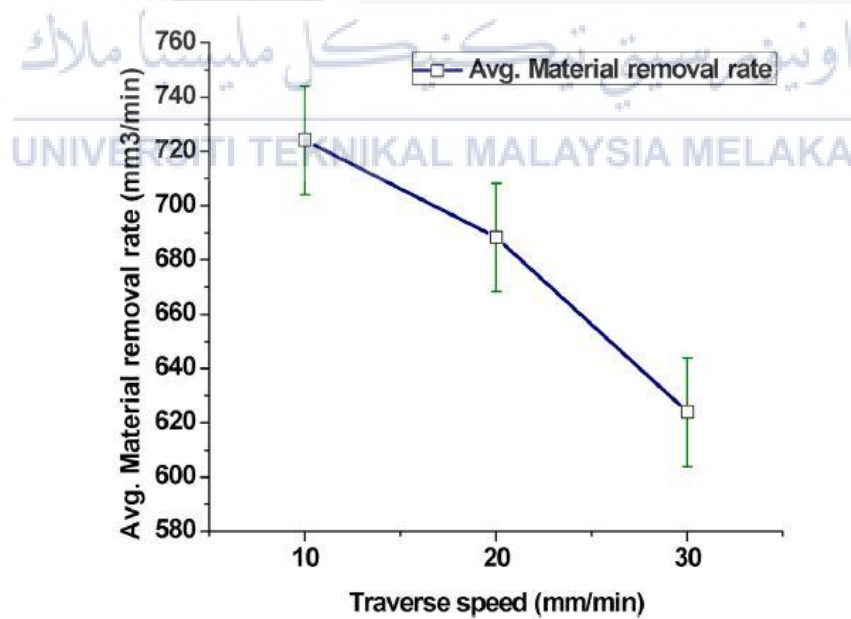
Figure 2.7: Material Removal Rate (MRR) Vs Traverse Speed (Srivastava *et al.*, 2017)

Table 2.3: The compilation feed rate parameter of AWJT from literature.

Author	Parameters/Methods	Findings/ Observations
Fuat *et al.* (2016)	Feed rate = 10-25 mm/min	Surface roughness increase when the feed rate increased from 10 mm/min to 25 mm/min
Srivastava *et al.* (2017)	Feed rate = 10, 20, 30 mm/min	The percentage of reduction in diameter decreased when the traverse speed increased from 10 mm/min to 30 mm/min.
M. El-Hofy *et al.* (2018)	Feed rate = 50, 150 mm/min	The value of kerf width increased when the value of pressure is high while the value of feed rate is low
	Pressure = 100, 350 MPa	
	Standoff distance = 2, 4 mm	Low feed rates and small stand-off distances result in excellent surface finish.
Uma Maheshwera *et al.* (2018)	Feed rate = 0.1, 0.2, 0.3 mm/rev	The value of surface roughness decreased when the rotational speed is increased at a constant feed rate
	Rotational speed = 100, 150, 200 m/min	

2.3.4 The effect of stand-off distance

Based on the result of Tarek *et al.* (2018), they found that stand-off distance is not a significant factor in creating a better surface finish on the product. The figure below shows that if the stand-off distance is smaller or higher, then the surface roughness does not show a significant range value. For example, the stand-off distance value of 2 mm (Run 1, 29 and 30) does not show any significant roughness on the surface.

14

Experimental data.

Run	Type	A: traverse speed (mm/min)	B: water pressure (MPa)	C: standoff distance (mm)	R_a (μm)
1	Axial	30.00	200.00	2.00	4.244
2	Axial	30.00	200.00	2.00	3.988
3	Fact	54.32	140.54	2.59	4.912
4	Fact	54.32	259.46	1.41	4.592
5	Fact	54.32	140.54	1.41	4.792
6	Fact	54.32	259.46	2.59	4.628
7	Fact	54.32	140.54	2.59	4.928
8	Fact	54.32	140.54	1.41	4.964
9	Fact	54.32	259.46	2.59	4.136
10	Fact	54.32	259.46	1.41	4.404
11	Axial	90.00	200.00	3.00	4.612
12	Axial	90.00	200.00	3.00	4.832
13	Axial	90.00	200.00	1.00	4.532
14	Axial	90.00	300.00	2.00	4.936
15	Axial	90.00	300.00	2.00	4.836
16	Center	90.00	200.00	2.00	4.632
17	Axial	90.00	100.00	2.00	4.088
18	Axial	90.00	200.00	1.00	4.56
19	Center	90.00	200.00	2.00	4.86
20	Axial	90.00	100.00	2.00	4.092
21	Fact	125.68	259.46	1.41	5.096
22	Fact	125.68	259.46	2.59	4.952
23	Fact	125.68	259.46	1.41	4.824
24	Fact	125.68	140.54	1.41	4.476
25	Fact	125.68	140.54	2.59	5.2
26	Fact	125.68	259.46	2.59	5.384
27	Fact	125.68	140.54	1.41	3.628
28	Fact	125.68	140.54	2.59	5.224
29	Axial	150.00	200.00	2.00	5.04
30	Axial	150.00	200.00	2.00	4.86

Figure 2.8: Experimental result (Tarek *et al.*,2018)

In addition, in order to develop a better surface profile, stand-off distance must be increased, based on the study by Balamurugan *et al.*(2018). Stand-off distance related to the effect of cavitations, especially when high-pressure levels hit the top of the surface decreasing. Balamurugan *et al.*(2018) also noted that the corresponding stand-off distance value is 10 mm. Figure 2.8 shows the SEM images for stand-off distance when 10 mm is used and two different nozzle angle values of 30˚ and 45˚, respectively. Table 2.4 showing the compilation stand-off distance parameter of AWJT from literature.
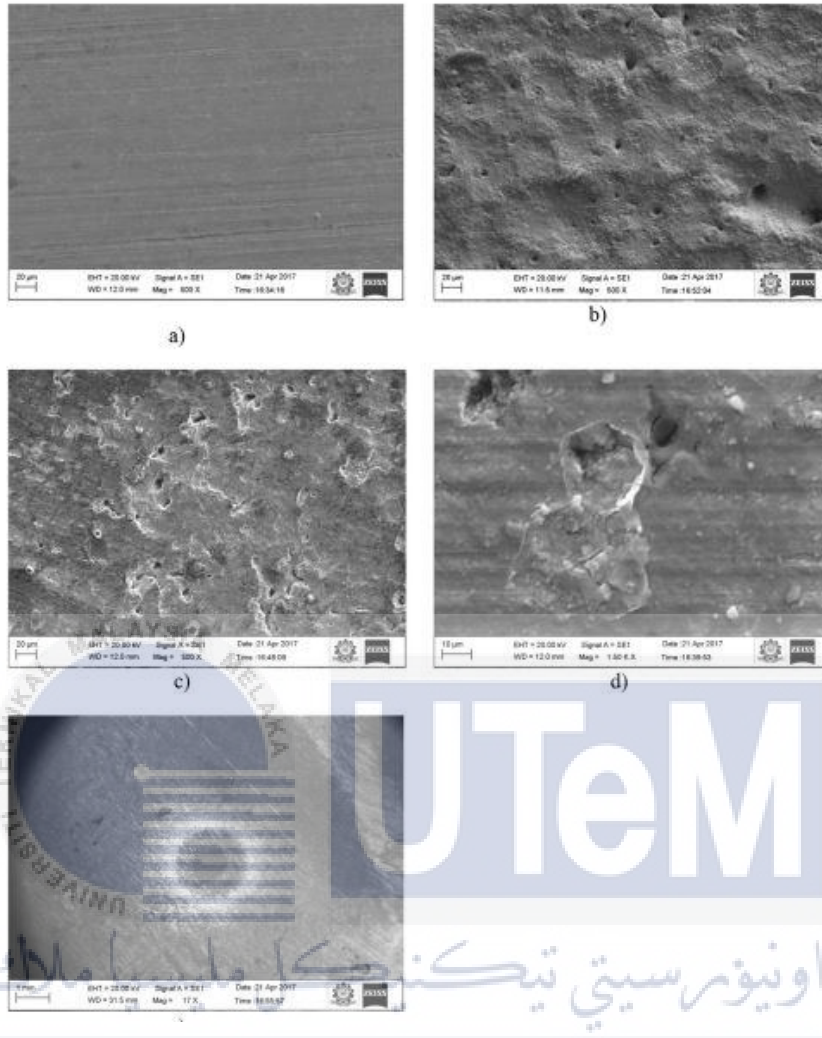
Figure 2.9: SEM imaged of unpeeled samples(a), Peened sample by stand-off distance 10mm and nozzle angle 30˚(b), peened sample by stand-off distance 10mm and nozzle angle 45˚(c), magnified view of the peened sample by stand-off distance 10mm and nozzle angle 45˚(d), strengthened zone of peened sample by stand-off distance 10mm and nozzle angle 30˚ (Balamurugan *et al.*,2018)

Table 2.4: The compilation stand-off distance parameter of AWJT from literature

Author	Parameters/ Methods	Findings/ Observations
Tarek *et al.* (2018)	Standoff distance = 1- 3 mm	Stand-off distance is not significant in producing a better surface finish.
Balamurugan *et al.*(2018)	Standoff distance = 10, 25, 60 mm	10mm is the corresponding of stand-off distance
N. F. Mohamad *et al.* (2020)	Standoff distance= 5, 8, 9, 10, 11, 15, 18, 20, 25 mm	Kerf taper increased when the value of stand-off distance increase from 8 mm to 18 mm.
Popan *et al.* (2017)	Standoff distance= 0.5, 1, 2, 3, 4, 5 mm	Stand-off distance is a major factor affecting the kerf geometry dimension.
		Stand-off distance is a minor factor affecting the surface roughness of the specimen.

2.4   Surface Roughness

Vivek *et al.*(2019), Rajesh and Srinivas (2017), and Tarek *et al.* (2018) explained that the length of scratches on the machined surface triggered by the abrasive particles increased when the traverse speed increased meanwhile the depth of the scratch decreases. They also found a better surface finish was achieved at higher traverse speeds. Figure 2.10 shows the size of scratches with three different traverse speed which is 1000 mm/min, 1400 mm/min and 1600 mm/min respectively. Rajesh and Srinivas (2017) also state that the surface roughness is influenced by the traverse rate of the water jet, where the surface roughness will increase when the traverse rate increases. They also found that to achieve the lower surface roughness and better surface finish, traverse speed must be lower, and it will increase the interaction of time between the abrasive water jet and unit surface area of the material.
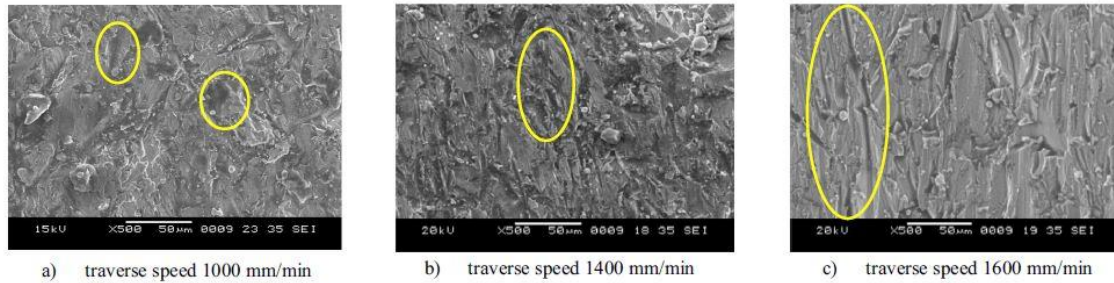
Figure 2.10: Scanning Electron Microscope(SEM) diagram of three different traverse speed (Vivek *et al.*,2019)

Besides, A. Alberdi *et al.* (2017) analyzed alloy 718 using an abrasive water jet found the similarity value of longitudinal and transversal average roughness. The tool path is not shown any other effect. They also found that the average roughness is obtained in the range of 9 µm to 15 µm. The same results are obtained in the study of abrasive water jet peening with elastic prestress by Sadasivam *et al.* (2009). The figure below shows the average roughness in terms of longitudinal and transversal average roughness.
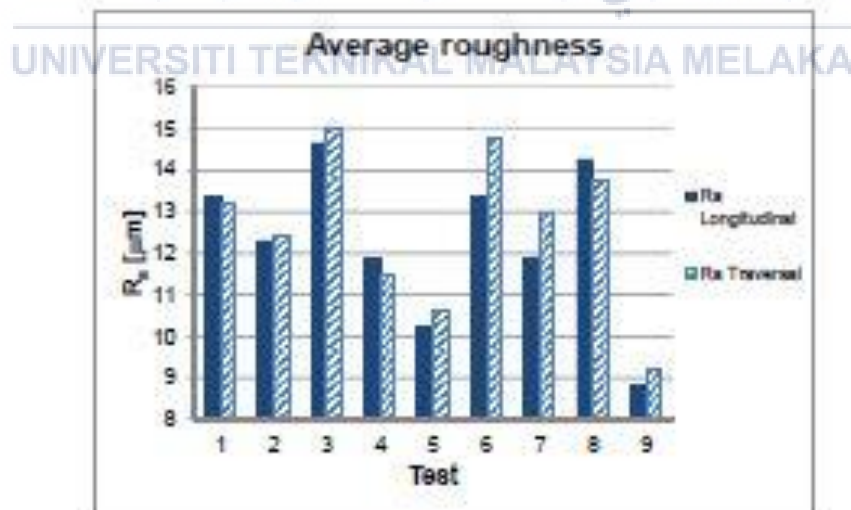
Figure 2.11: The average roughness in terms of longitudinal and transversal average roughness(A. Alberdi *et al.*,2017).

18

Hlavavek *et al.* (2015) revealed that the workpieces' final surface quality is also influenced by the direction of rotation for the workpieces. This is based on their investigation of the effect of traverse speed, rotational speed, and the direction of rotation on the surface quality of sandstone workpieces with AWJT. As demonstrated in Libor Sitek and Petr Hlavacek's (2016) observation, the rougher surface is obtained when the workpiece direction rotates toward the jet nozzle (opposite to jet nozzle). Figure 2.12 shows the workpiece direction rotation effect. The same observation is obtained on Hashish (2016) experiments. Hashish (2016) found that when the workpieces are turned negatively, the surface waviness in the workpieces is greater. Then, there is also a greater relative velocity between the jet and the workpieces. If the workpieces are turned in a positive direction, chips and abrasive particles are more effectively removed. Figure 2.13 shows the difference between two different rotations directional and the occurrence of surface waviness when the workpiece is being cut.

Figure 2.12: The effect of workpiece when the rotational direction against the direction of water stream
(Libor Sitek and Petr Hlavacek,2016)

19
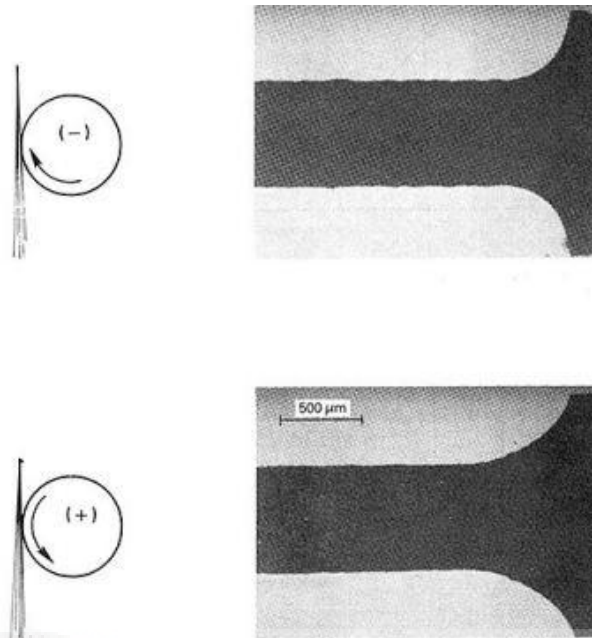
Figure 2.13: The difference between two different rotations directional and the occurrence of surface waviness (Hashish,2016)

Abrasive flow rate is one of the essential factors in AWJT machining. According to Fuat *et al.*'s (2016) research, the average surface roughness decrease when the amount of the abrasive flow rate increase (Figure 2.14). They also observed that a smoother surface of the workpiece is obtained when the workpieces receive the impact of the pressured water and abrasive which mixed in the chamber mixing will produce high quality or state of being homogenous.

20
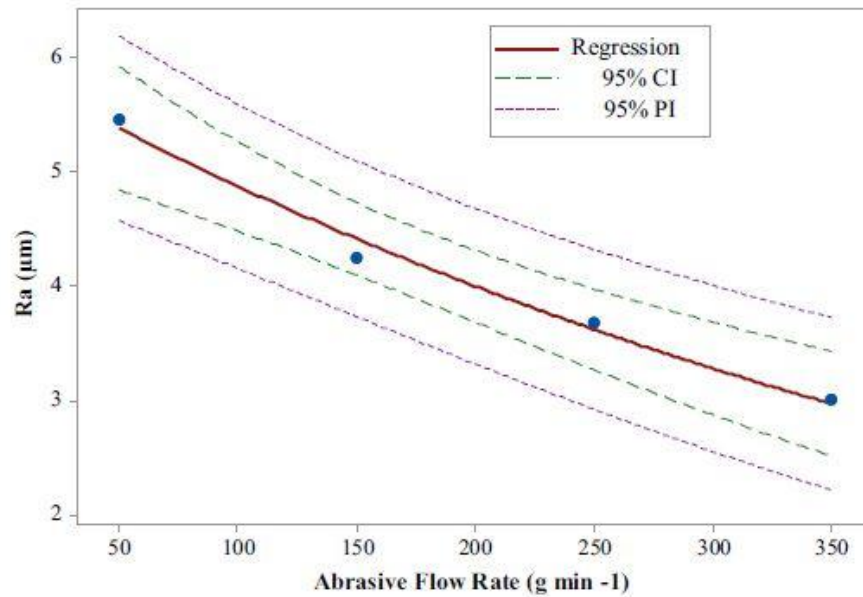
Figure 2.14: Effect of abrasive flow rate on the surface roughness (Fuat *et al.* (2016)

Weiyi *et al.* (2013) conducted a study of the effect of process parameters on the MRR and depth of cut. One of the parameters involved is the abrasive flow rate. They point out that a higher rate of abrasive flow rate is connected to more abrasives that may hit each other, thus causing large quantities of kinetic energy to be wasted. The figure below shows that the DOC is influenced by the pressure of 380 MPa and 200 MPa and abrasive flow rate. For 380 MPa, the parabolic trend is obtained while for 200 MPa, the trend is slightly decreased. They also observed that supplying more abrasive, would increase the ability to remove more material.
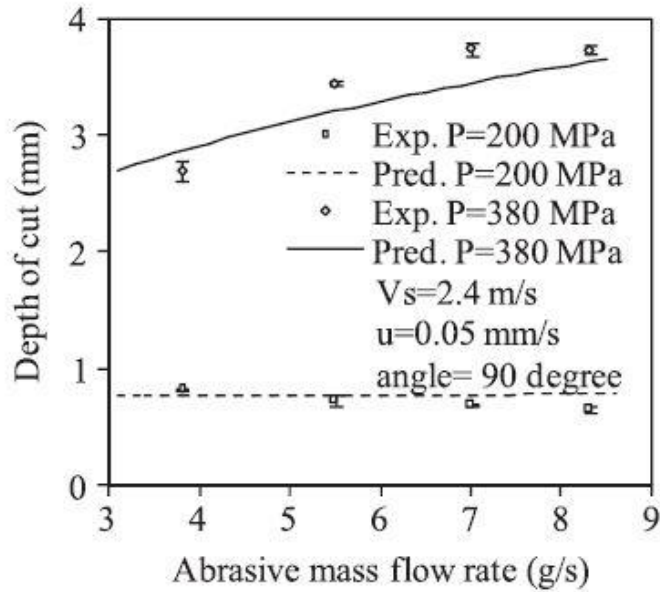
Figure 2.15: Effect of abrasive flow rate on DOC (Weiyi *et al.*,2013)

Weiyi *et al.*(2013) also observed the effect of abrasive flow rate on surface roughness. They found the depth of cut and surface roughness has a bond that is easy to understand because surface roughness is mostly affected by the undercuts formed in the second cutting zone. Based on Eckart *et al.* (2012)'s analysis, the highest material removal rates are achieved when the average surface roughness, Ra is 50.8 µm (Figure 2.16) with several parameters is constant which is pressure, feed rate, jet impact angle, and abrasive flow rate. Besides, D.R. Tripathi *et al.* (2020) revealed that the most parameters that influenced MRR value are the cutting speed and abrasive flow rate. They also observed that the optimum value for cutting speed and the abrasive flow rate is 100 cm/min and 300 cm/min, respectively.
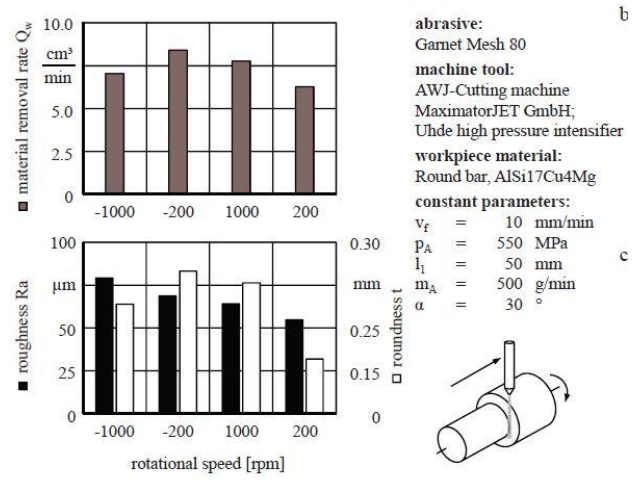
Figure 2.16: Difference between material removal rate and roughness of specimens (Eckart *et al.*,2012)

2.5 Dimensional Accuracy

2.5.1 Roundness

The circular shape of the Inconel 718 Alloy specimen is closely related to roundness measurement, which depends on several factors in the abrasive water jet turning such as stand-off distance, traverse speed, abrasive flow rate, and others. Kumar *et al.* (2017) observed that although other factors are constant, the traverse speed plays an important factor in obtaining the specimen's desire circularity. On the other research by A. C. A. Raj *et al.* (2018), they identify that stand-off distance is the major effect in the value of roundness. They also identify that the roundness value increased when the water pressure increased and indirectly increased the surface quality. C. A. Sari *et al.* (2018) defined the formula for roundness value in (1).

23

$$R = \frac{4\pi A}{p^2} \tag{1}$$

Where, R = Roundness

A = Area

p = Perimeter

2.5.1.1 Eccentricity

Eccentricity is known as the center position of a profile relative to some point of datum. Eccentricity is a vector quantity that contains magnitude(the center of reference circle) and direction (angle from the datum point). The value of eccentricity is obtained by using the comparison of the distance of the foci ellipse minor, and the foci ellipse major an object (C. A. Sari *et al.*,2018). C. A. Sari *et al.* (2018) observed that the round of object has an eccentricity value close to 0 while for an elongated object or square shape, the eccentricity value between 0 and 1. They also defined the formula of eccentricity in (2).

$$e = \sqrt{1 - \frac{b^2}{a^2}} \tag{2}$$

Where, e = Eccentricity

b = Minor axis

a = major axis

H. H. Tian *et al.* (2020) revealed that difficult to control the value of eccentricity with the large radius because it can cause roundness measurement distortion. They also revealed

24

that the higher value of eccentricity could maintain the accuracy of roundness measurement and concluded that the error value of roundness is directly proportional to the square of the eccentricity.

Figure 2.17: The model of roundness and eccentricity (H. H. Tian *et al.*, 2020)
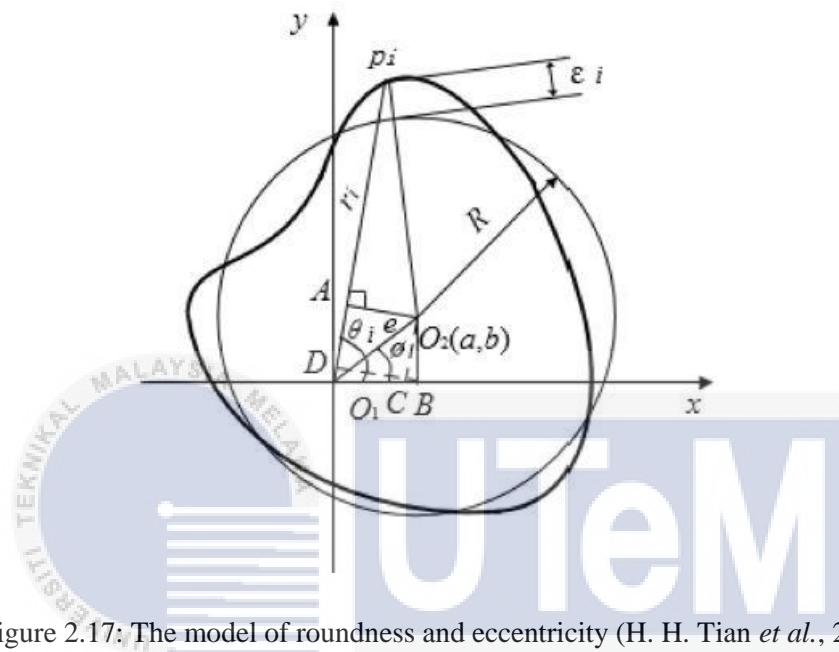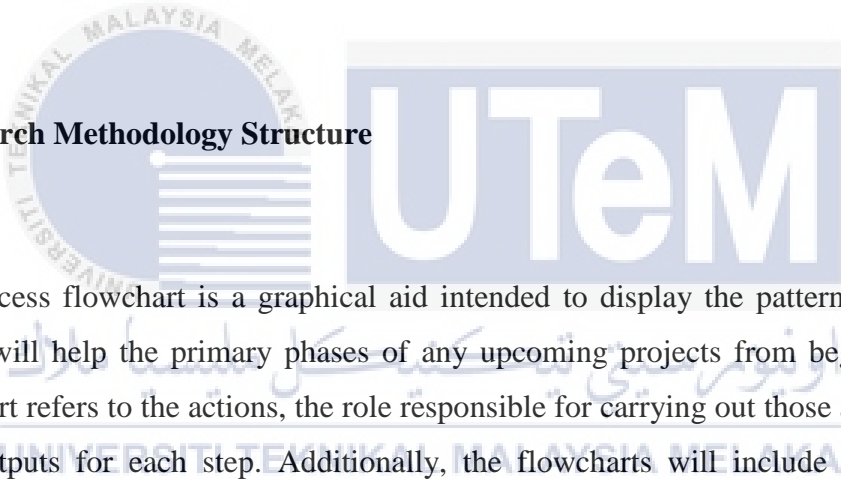
CHAPTER 3

METHODOLOGY

3.1   Research Methodology Structure

A process flowchart is a graphical aid intended to display the pattern of steps to be followed. It will help the primary phases of any upcoming projects from beginning to end. Each flowchart refers to the actions, the role responsible for carrying out those actions, and the input and outputs for each step. Additionally, the flowcharts will include records of any documents and other materials necessary to carry out activities.

Based on the objective of the experiment, three phases carry out the primary process of this experiment. The first phase is the literature review research. The information and the data collected in the literature review must be parallel with the project's objective. The second phase, after all, objective accomplished, is to reduce the dimension of Inconel 718 material by using AWJT. This method focuses only on the AWJT parameter, which is a feed rate, rotational speed, and depth of cut. After that, the parameter will be optimized by using the Full Factorial design in DoE. A surface roughness machine is used to figure out the surface characteristic of the Inconel 718 alloy, while a roundness machine is used to identify the value

of roundness and eccentricity of Inconel 718 alloy after machining. The final phase is analysis, and data collection is obtained to ensure success and proof of the research.
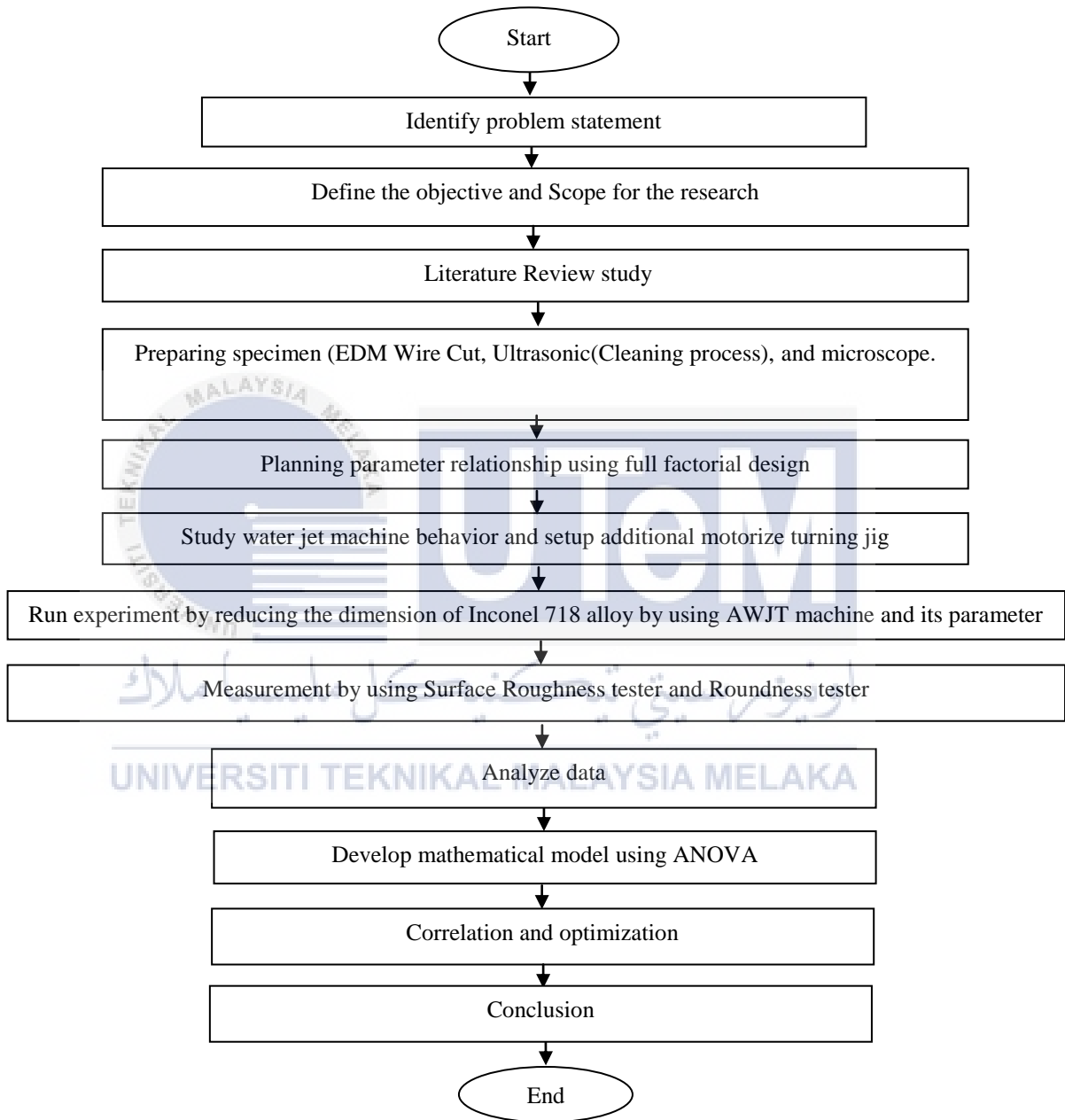
Figure 3.1: Flow chart of process methodology

3.2 Preparation Tools

3.2.1 Electrical Discharge Machining (EDM) wire cut

Electrical Discharge Machining (EDM) Wire Cut machine uses a small diameter of wire that will be energized by using electrical power to slice the workpieces based on the required size. EDM Wire Cut also can provide accurate dimensional for close-fitting parts. In EDM Wire Cut, the water acts as a dielectric fluid, control resistivity and other electrical properties with filters and de-ionizer units. Water drains out the debris that has been cut from the cutting zone. Basically, EDM Wire Cut is mostly used when low residual stress is desired. It is because it does not require high cutting forces for the removal of material.

Figure 3.2: Electrical Discharge Machining (EDM) Wire Cut

3.2.1.1   Procedures of EDM wire cut machine

There are three main steps while handling the EDM Wire Cut machine:

1. Master CAM program

    - Set up the setting of the EDM Wire Cut Machine.

2. Updates program

    - Make sure the right program is used.

3. Machining the samples

    - The workpieces must parallel with the work table and ensure the screw is tight.

    - All the information, such as the size of the wire, the type of wire, and others is correct.

3.2.1.2   Safety precaution

- There are no leaks in the dielectric fluid tank hose and pipe connection.

- Installed the material in the area where the process is run.

- The wire of EDM Wire Cut is not touching the workpieces.

- Make sure all the cables are no leakage.

- Wear appropriate clothing during the machining process.

3.2.2 Ultrasonic cleaning process

Ultrasonic cleaning is the process where the sound of waves is used to remove contamination particles from the surface of the sample. By using the ultrasonic process, the original specification of the material characteristic is obtained. The ultrasonic process is started by submerging the part into an ultrasonic bath after unwanted contaminants and debris is removed. After using an ultrasonic process, various particles can permeate the surface of the metal. Contaminants, debris, and other particles such as free iron, grease, and machining oils may affect the strength of the natural surface and may be embedded in the surface during the machining process.

In this process, the product will have smooth appearances, cleanliness, and improved and extended life. Finally, it is important to admit that the ultrasonic process does not change the outward appearances of the base metal.

Figure 3.3: Ultrasonic Cleaning

3.2.2.1   Procedures of ultrasonic cleaning

There are several steps involves to conduct Ultrasonic Cleaning process:

1. Make sure the drain of the ultrasonic machine is closed.
2. Turn on the switch of the ultrasonic bath.
3. Add ethanol solution in a measuring cylinder of the appropriate size until the sample is submerged.
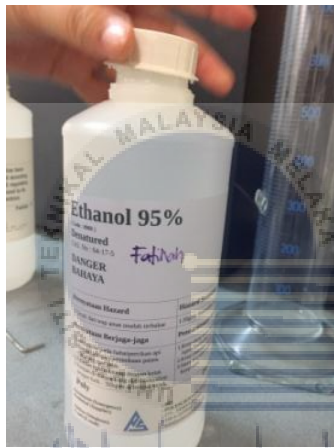
4. Place the measuring cylinder in the ultrasonic bath and set the temperature at 27° at 15 minutes.
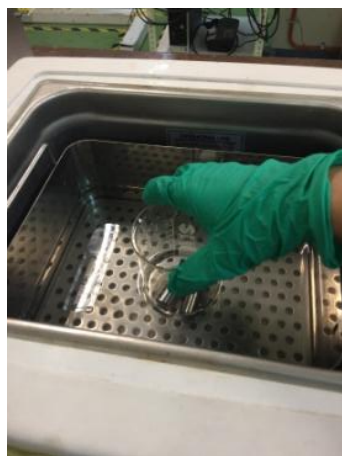
5. After that, rinse the sample by using distilled water.

6. Dry all the samples.

3.3   Experimentation

3.3.1   Abrasive Water Jet Turning(AWJT) machine

AWJT is the alternative to replace conventional turning, which is a lathe machine. Conventional turning has a lot of issues, especially in tool life, surface finish, and productivity. In the AWJT, the air is compressed used to transport the abrasive particles in the compressor and is stored in the reservoir. The flow fluctuations are removed in the abrasive tank, and the air stored in the abrasive tank is fed into the system through a pressure regulator. The pressure regulator will maintain a constant pressure. The mixing of the abrasive particles with the high-pressure water takes place in the mixing chamber. The combination of abrasive particles and high-pressure water is directed through the nozzle to remove material from the workpieces.
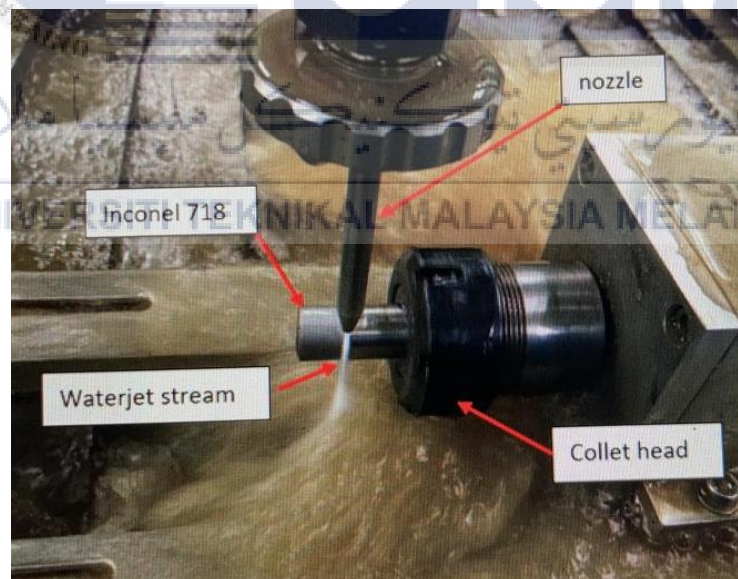
Figure 3. 4: Machine setup

Figure 3.5: AWJT machine

3.3.1.1   Procedures of AWJT machine

3.3.1.1.1   Machine Procedure
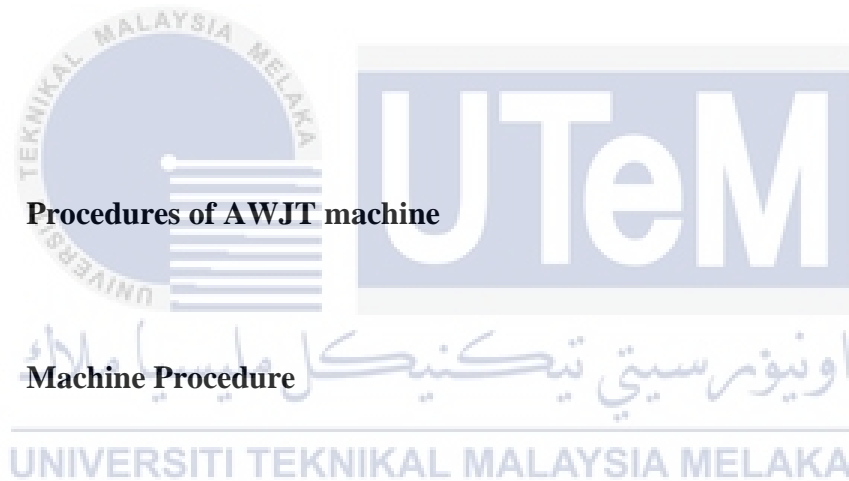
There are several steps to set up the AWJT machine, which is:

    i.   The pump is switched on, ensuring the abrasive tank and chiller must be lower than 20˚C before the machine is switched on.

    ii.   All emergency buttons are released.

    iii.   The machine, air compressor, water tank pump, and air dryer are switched on.

    iv.   The transparent door at the water chiller opens and switched on the green button.

    v.   The top cover is opened to check the abrasive hole is tightly closed with rubber. The rubber is pulled out till no abrasive or air going out.

    vi.   Then, the AWJT machine is ready.

3.3.1.1.2 Installing Jig

There are several steps to install the jig of the AWJT machine, which is:

    i.   Leveling using water level, please note that if not level or not center. Added plate and re-measure it several times. (Figure 3.6)

    ii.   Then, the jig is clamped, and the distance of the jig and waterjet table is measured.

    iii.   Ensure the connecter wire on the motor is always wrapped neatly so that it is not exposed to water.

    iv.   Specimens are clamped tightly using a suitable vice/jig/clamp.

    v.   The software flow cut is opened and makes a home position for the Z-axis, X-axis, and Y-axis.

    vi.   All the connection is checked and make sure abrasive flow smoothly. Run a test run first outside the specimen before starting the cutting process.

    vii.   After the jig is clamped, the laser button at the water level is switched on, and see the bubbling water in the middle to make sure all the diagonal X and Y are not tilted.

    viii.   The air compressor opens then blows in the jig.

    ix.   The motor is installed.

Figure 3.6: Leveling using water level

35
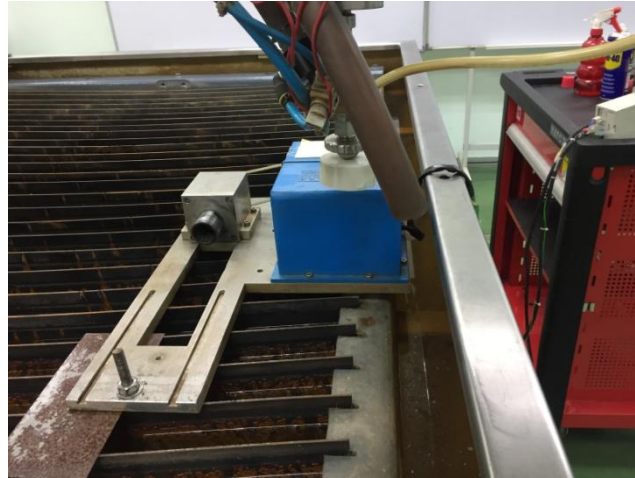
Figure 3.7: Installing jig

3.3.1.1.3 Dial Test Indicator (DTI)

Before performing the experiments, the digital dial indicator gauge (Figure 3.8) is used to show the run-off which is the misalignment between the rotational symmetry axis of the workpiece and the movement axis of the nozzle to measure linear movements with high accuracy. The precision of the die indicator is 0.001 mm or 1 μm.

Figure 3.8: Digital Dial Indicator Gauge

Figure 3.9: Dial tester indicator

3.3.1.1.4   Zeroing and positioning

There are several steps involved in zeroing and positioning, which is:

i.   Z-axis, X-axis, and Y-axis is set in machine home

ii.   20mm collet of edge finder that has 20mm shank diameter is used.

iii.   The edge finger is inserted in the slot. Then the flow cut file is open to adjusting the positioning

iv.   Positioning the probe to Z=0 and Y=0.

v.   The coordinate for Z-axis is taken after the accurate value is obtained. (Use "Page Up" for moving up (+) and use "Page Down" for moving down (-))

vi.   The coordinate for Y-axis is taken after the accurate value is obtained. (Use "Arrow Up" and "Arrow Down" for moving).

vii.   The coordinate for X-axis is taken after the accurate value is obtained. (Use "Arrow Right" and "Arrow Left" for moving).

viii.   Set home as current position 1.

ix.   Uninstall the edge finder from the collect head and split the 20mm collet.

x.   Then attach the 16 x 50 mm specimen to collect 16 mm, make sure the workpiece is overhanging 30 mm, and tighten it into the collet head.

xi.   The experiment was started based on DOC, which is 0.1 mm and 0.3 mm.

Figure 3.10: Zero position of Y-axis by using an electronic edge finder
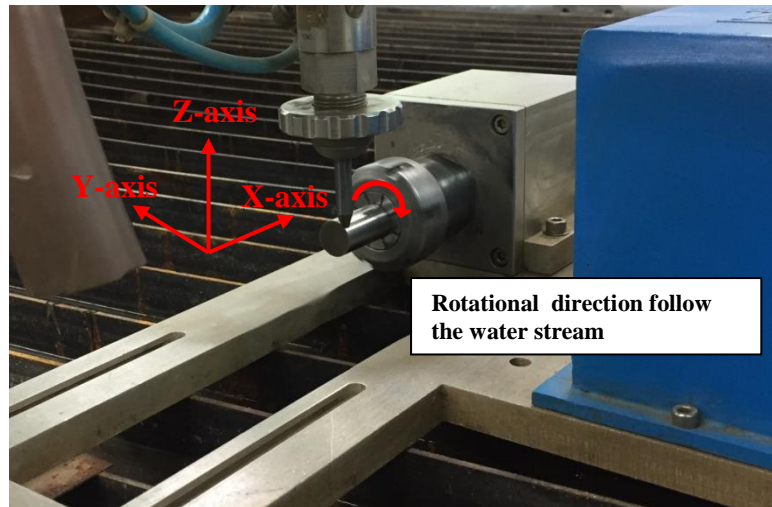
Figure 3.11: Zero position of the workpiece
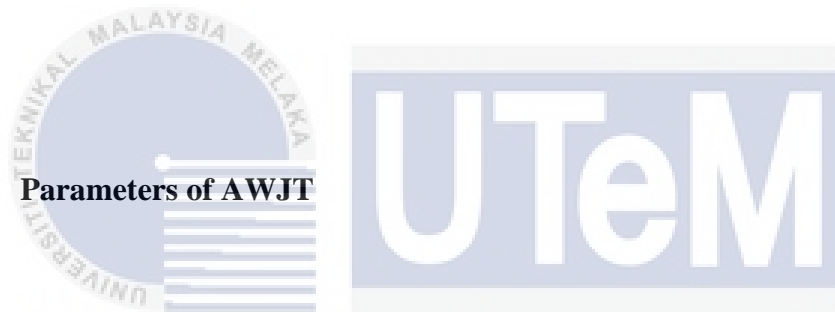
3.3.1.2   Parameters of AWJT

All experiments will be performed on the AWJT machine with the specification as shown in Table 3.1.

Table 3.1: Specification of AWJT machine

Specification	Description
Model	Flow-March 2b
Traverse range	Up to 10 m/min
Linear straightness accuracy	± 0.07 mm/m
Water pressure	400 MPa
Water velocity	4.116 x 10^7 mm/min
Repeatability	± 0.060 mm

3.3.1.3   Abrasive particles- Garnet mesh size 80

Garnet sand is a famous material in AWJ machining due to its advantages on high specific weight. Thus, garnet sand develops minimum dust during the process. Besides, this sand can also be used in different industries and can be reused more than five times. Garnet sand is categorized as silicate minerals. In this project, the type of garnet mesh size 80 will be used to complete the project.
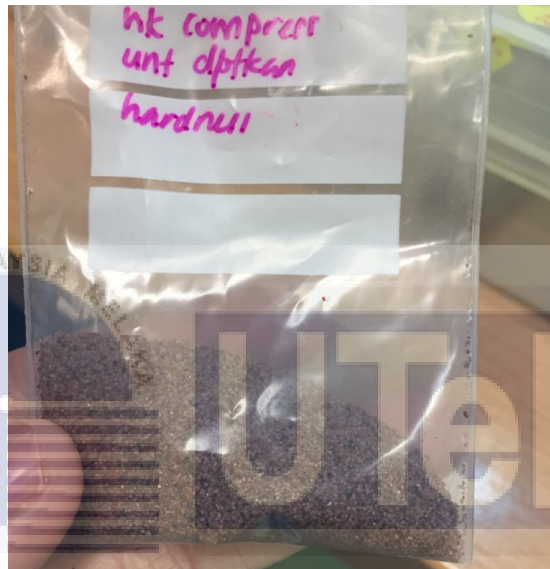
Figure 3.12: Abrasive garnet mesh size 80

3.3.1.3.1   Physical characteristics

The table below shows the physical characteristic of the material abrasive, which is garnet sand.

Table 3.2: Physical characteristic of garnet sand mesh size 80

Physical Characteristics	Values
Specific gravity	4.1 g/cm^3
Hardness	>7 moh scale
Acid Solubility	<1.0%
Colour	Red-pink
Conductivity	<150 µS/cm
Chloride	<25 ppm
Grain shape	Subangular
Toxic Substances	None
Moisture	0.1-7%
Bulk density	2.47 g/cm^3

3.3.1.3.2 Chemical analysis

Table 3.3 shows the element that involved the material abrasive particle that will be used on the AWJT machine, which is garnet sand.

Table 3.3: Chemical analysis of garnet sand mesh size 80

Element	Percentage (%)
SiO_2	37.15
Al_2O_3	21.04
Fe_2O_3	30.38
MnO	7.24
CaO	1.33
TiO_2	1.42

3.3.2 Inconel 718 alloy

Inconel 718 alloy is known as a nickel base that is commonly used to construct a turbine's part in aerospace engineering. Inconel 718 alloy is superalloys that have the ability to

be a machine at high temperatures. Superalloys can be classified into three groups consisting of nickel base, cobalt base, and iron nickel-base alloys. Only a nickel base is widely used, particularly in power generation turbine components, aerospace engines, and others. There are 8 samples with a diameter of 16 mm and a length of 50 mm. Figure 3.13 shows the specimen throughout experiment.

Figure 3.13: Inconel 718 alloy specimen

3.3.2.1   Mechanical properties

Table 3.4 shows the mechanical properties of the Inconel 718 alloy that will be used on the AWJT machine.

Table 3.4: Mechanical properties of Inconel 718 alloy

Mechanical properties	Value
Ultimate tensile strength	1375 MPa
Yield strength	1100 MPa
Elongation	25%

3.3.2.2 Thermal Properties

Table 3.5 shows the thermal properties of the Inconel 718 alloy that will be used on the AWJT machine.

Table 3.5: Thermal properties of Inconel 718 alloy

Thermal properties	Value
Specific heat capacity	0.435 J/g-˚C
Thermal conductivity	11.4 W/m-k
Melting point	1260˚C - 1336˚C
Solidus	1260˚C
Liquidus	1336˚C

3.3.3   Nozzle size

The nozzle used was 76.2 mm in length, and the orifice used was 0.25 mm in diameter (Figure 3.14). The schematic diagram of the nozzle is shown in Figure 3.15. The working pressure for this nozzle is 400 MPa. It is a service life of up to 200 hours. A tiny orifice made of very hard material such as sapphires 6 (usually with a hole of a few hundred micrometers in diameter) is used to produce a high-speed compressive waterjet in the nozzle.

Figure 3.14: Nozzle
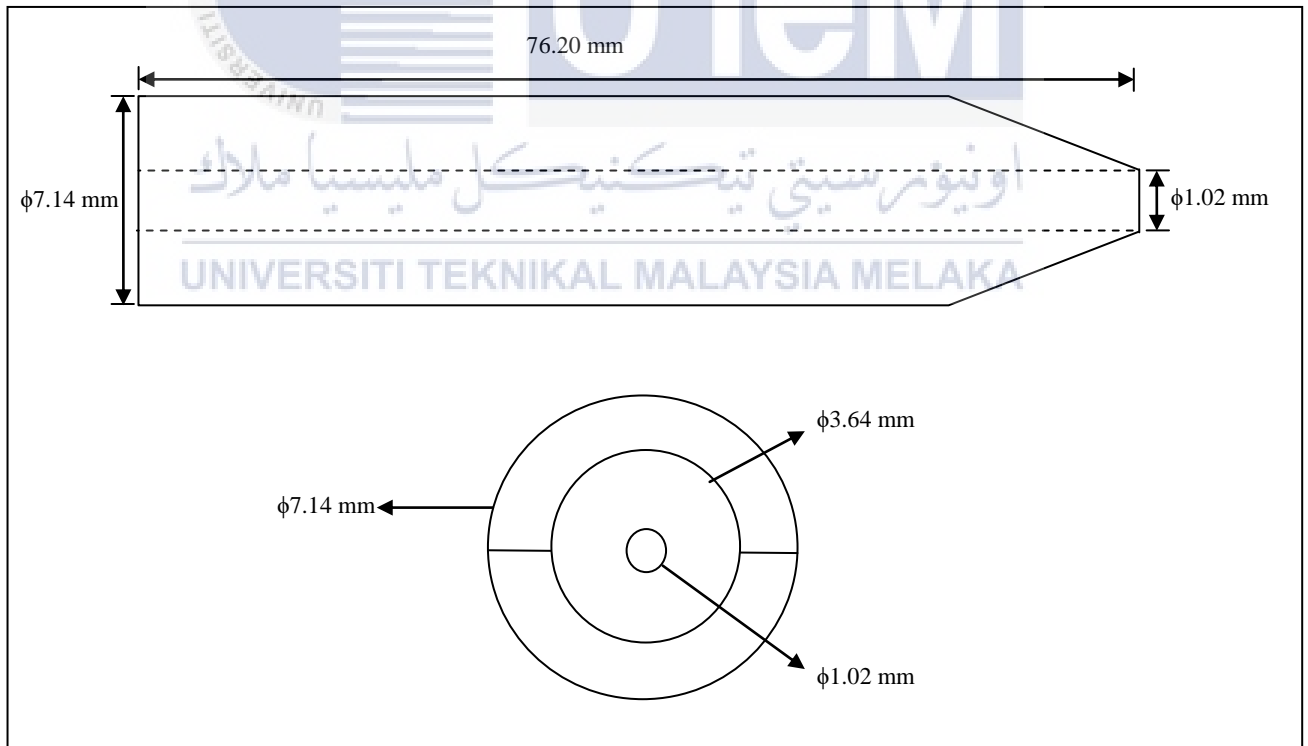
Figure 3.15: Schematic diagram of the nozzle

3.3.4 Pilot testing

A pilot test is a crucial stage at the beginning of the researchers to identify potential problem areas in the research instrument to complete the study. It is also defined as a small-scale experiment to test data collection instruments, sample recruitment strategies, and others. A pilot testing could address several logistical challenges such as:

- Equipment operation in the correct manner, or not.
- Checking reliability and validity results.
- Determine study protocol feasibility and identify weaknesses within a study.
- Determine the initial data for the main result size and identify how many samples are required to complete this study.
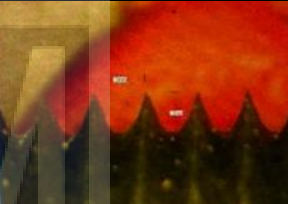
Pilot testing is an efficient method to discover the essential problems in the main study and help the researcher take corrective action to improve the research process. Connelly and L. M. (2008) suggest that the optimum sample projected for the pilot studies is around 10 %. Based on the research carried out by Hertzog, there are a lot of factors that influence the pilot studies, and this method is not transparent and forthright to find the solution to the problem. The table below shows the random sample of three different values for feed rate (Vt). The ratio is calculated by using the following equation (3).

$$Ratio = \frac{V_{stream}}{V_{traverse}} \tag{3}$$

Where, V_{stream} = Water direction(z-axis)

$V_{traverse}$ = Feed rate of the abrasive water jet (x-axis)

Table 3.6: The example of pilot studies

N(rev/min)	V stream Vs(mm/min)	V traverse Vt (mm/min)	V/N micron F (mm/rev)	V/Vs Ratio	Observation
60	4.116×10^7	3	0.05	13.72×10^6 Pitch invisible	
60	4.116×10^7	21.26	0.35	1.94×10^6 Watermark	
60	4.116×10^7	80.59	1.34	0.51×10^6 Thread	

3.3.5 Fixed and variable parameters

All the ranges of the parameter involved in the input variable are shown in Table 3.7. The range value of feed rate is collected from the results of the pilot test which is no watermark appear on the surface of the specimen.

46

Table 3.7: Fixed and variable parameter of AWJT machine

	Parameter	Value
Variable parameters	Depth of cut, ap	0.1 mm - 0.3 mm
	Feed Rate, f	1 mm/min - 3 mm/min
	Rotational Speed, N	60 rpm - 90 rpm
Fixed parameters	Stand-off distance, z	8 mm
	Surface distance	20 mm
	Jet angle	90˚
	Water pressure, P	340 MPa
	Water velocity	4.116×10^7 mm/min
	Rotational direction	Clockwise

3.3.6   Parameter process

The combination parameter will develop by using Design Expert Software to analyze the surface roughness of Inconel 718 Alloy and the dimensional accuracy.

3.3.6.1   Design of Experiment (DoE) method- Full Factorial

A full factorial design is a design that is widely accepted in manufacturing industries at 2-levels and 3-levels. The full factorial design explores several relationships between variable explanatory and more than one response variable by using Design Expert Software.

Figure 3.16: Design Expert Software

3.3.6.1.1 Procedure of DoE

Several steps involve conducting Full Factorial design:

1. Select the number of factors for the experiment.
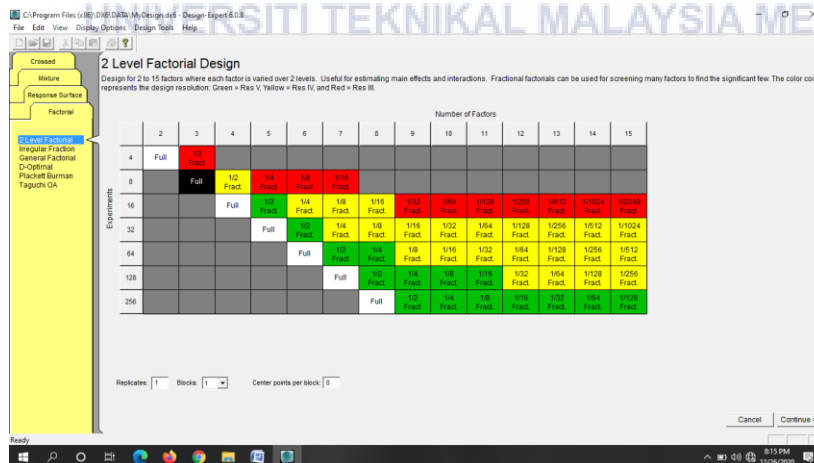
2. Select the input variables; Depth of Cut (DOC), Feed rate (f), and Rotational Speed (N). The names and levels are shown in the following figure.

3. Insert the value for each independent variable in the following figure.

4. Assign the total responses (output) of the project. On this project, there is three response which is surface roughness, roundness, eccentricity, and dimension error.
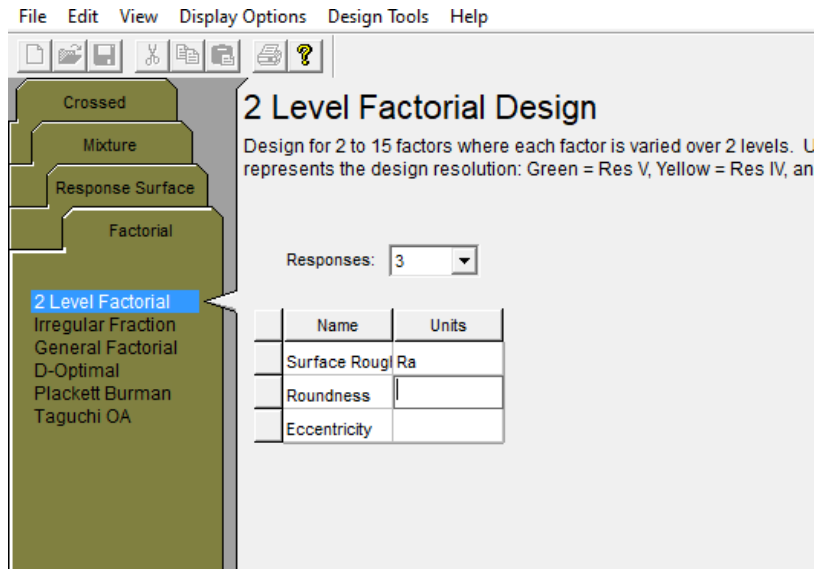
5. The experiments will be conducted and all the response data will be collected during the experiment.

6. The data of the experiment will be analyzed.
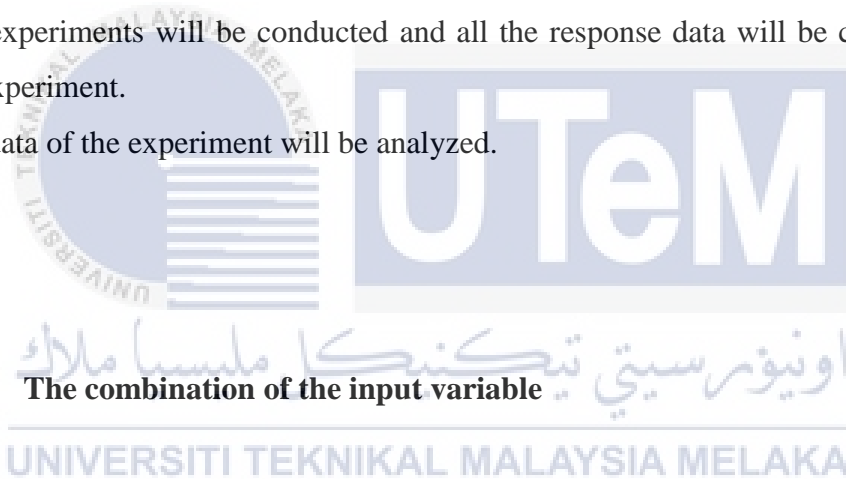
3.3.6.2   The combination of the input variable

Table 3.8 shows the input variable between feed rate, rotational speed, and depth of cut on eight samples of Inconel 718 alloy.

Table 3.8: The combination of the input variable (Feed rate, Rotational Speed and DOC) for eight samples

Run	DOC (mm)	Feed rate (mm/min)	Rotational speed (rpm)	Surface Roughness (µm)	Roundness (µm)	Eccentricity (µm)	Dimension error (mm)
1	0.3	1	90				
2	0.1	3	60				
3	0.3	1	60				
4	0.1	1	90				
5	0.1	1	60				
6	0.3	3	90				
7	0.1	3	90				
8	0.3	3	60				

3.4 Calculation

AWJT machine needs to operate manually to obtain accurate coordinates for the x-axis, y-axis, and z-axis. The axis for this machine is defined as shown in Figure 3.17. In this experiment, there are two different values for depth of cut, which is 0.1 mm and 0.3 mm, where the stand-off distance is fixed at 8 mm. Standoff distance is known as the distance from the surface of the specimen to the tip of the nozzle.
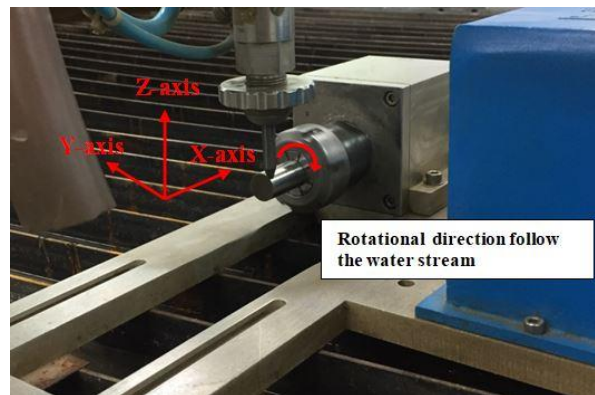
Figure 3.17: Coordinate system of 3 axis water jet machine

51
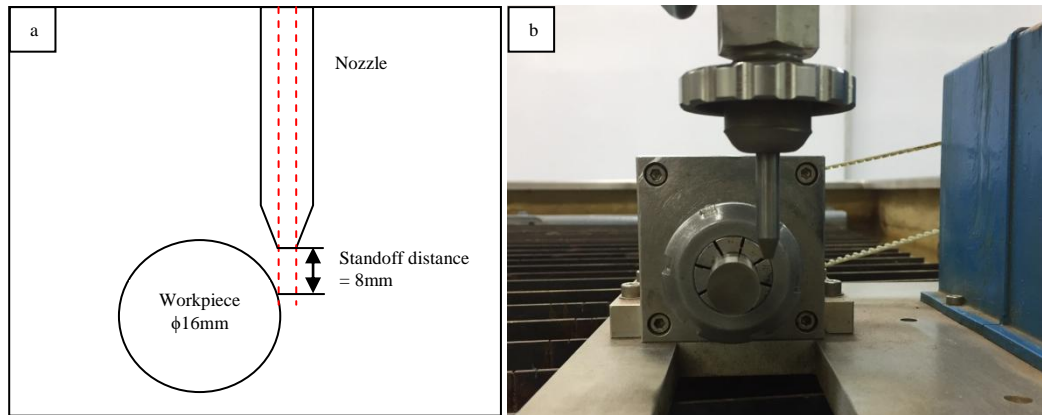
Figure 3.18: Stand-off diagram (a) Schematic diagram of stand-off distance (b) The position of the nozzle with stand-off 8mm

3.4.1   Calculation of DOC

The variable of DOC gives an impact on another axis, such as the x-axis and y-axis, due to the fixed value of stand-off distance, which is 8.0mm. Table 3.9 shows the zeroing axis of the AWJT machine. This machine needs to be careful during handling due to AWJT machine is fully manual.

Table 3.9: Zeroing value of AWJT machine

Position	Value
X-axis (x_1)	67.529
Y-axis (y_1)	213.557
Z-axis (z_1)	116.275

Pythagoras theorem method should be used to calculate the equation for the value of DOC. The formula of the Pythagoras Theorem method is defined in (3). Table 3.10 shows the new value for the y-axis and z-axis for DOC 0.1mm and 0.3mm with a fixed stand-off distance

52

with is 8.0mm by using the formula defined in (4). The position for the x-axis is using the same value because the surface distance (cutting flow) is 20mm.

$$c^2 = b^2 + c^2 \tag{3}$$

$$a = \overline{} \tag{4}$$
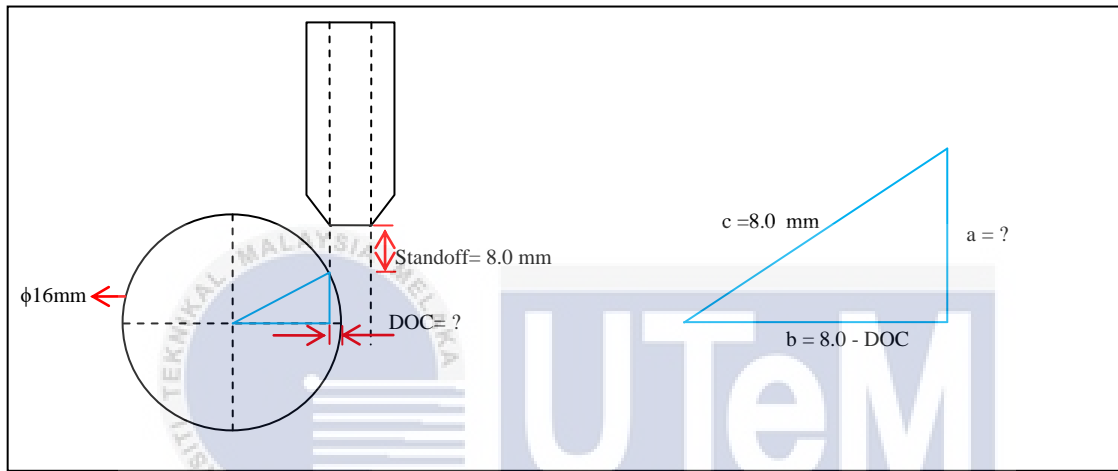
Figure 3.19: Schematic diagram for the variable of DOC with fixed stand-off distance

Table 3.10: New value for the position of the x-axis, y-axis, and z-axis

DOC	New Position	New Value
0.1	x_1	67.529
	y_2	$y_2 = y_1 + 0.100$
	z_2	$z_2 = z_1 - 1.261$
0.3	x_1	67.529
	y_3	$y_3 = y_1 + 0.300$
	z_3	$z_3 = z_1 - 2.710$

3.5   Measurement Tools

3.5.1 Surface roughness machine

Surface roughness machines are ideal for testing with enhanced capabilities, which means improved productivity when measuring surface roughness in any direction, including vertical and inverted. It also permits easy measurement in a variety of situations and settings. The function of the Portable Surface Roughness tester is to detect the amplitude and frequency to ensure that a surface is fit for a purpose. Caution while handling/operating this equipment is to make sure the drive unit is level with the precision roughness specimen.
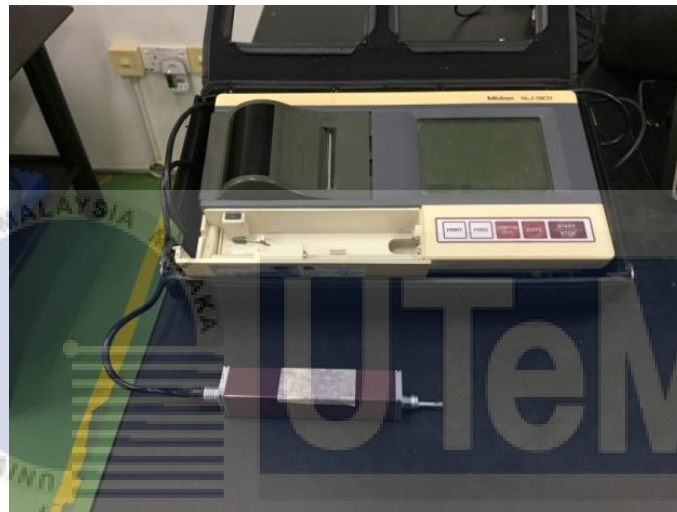
Figure 3.20: Surface Roughness machine

3.5.1.1 Procedure of surface roughness machine

There are four main steps involved during handling Surface Roughness Machine:

1. SJ-301 Preparation

    • Switch to main power after all the wire is connected to the right place.

2. Performing Calibration

- Ensure the detector stylus is parallel to the measured surface.
- Compare whether the nominal value is the same as that printed on the precision roughness samples.

- Press the "start" to perform the work while pressing the "stop" to stop the calibration process.

3. Measurement

- Position the sample of Inconel 718 alloy and make sure the detector stylus is parallel to the surface of the sample.

- After the measurement has been completed (Five reading covering five random different spots is obtained for each specimen before getting the average reading), touch the scroll parameter to display the required parameter.

4. Printing Measured Result

- Press the "print" button on the display unit after the measurement has complete.

3.5.2 CNC Roundness Measuring Machine

In this study, Mahr MMQ 44 CNC will be used to run the roundness measurement. The component is rotated on a highly accurate spindle which provides a circular datum. The workpiece axis is aligned with the axis of the spindle through a leveling table. During rotation, a transducer measures radial variations of the component concerning the spindle axis.

3.5.2.1   Procedure of CNC Roundness Measuring Machine

The step involved while handling the roundness measuring cylinder:

1. The workpiece is placed on the center of roundness's rotary able axis.
2. Adjustment prior to leveling as any inclination of the workpiece's axis must be sufficiently parallel with respect to the rotary axis of the measuring apparatus. Figure 3.21 shows the z-axis of measurement known as the length from the table work of the roundness tester.
3. Set the effect of filter variation of cutoff value on measurement profile either no filter, low-pass filter, or band-pass filter.
4. Evaluate the measurement profile roundness input to develop remark circles whose measurement value is described.
5. Choose stylus tip of roundness machine as requirement needs to measure such as ball type, cylinder type, axe type or egg type, tip radius, and measuring forces.
6. The undulation of data per revolution (UPR) in roundness graphs to indicate the UPR condition.
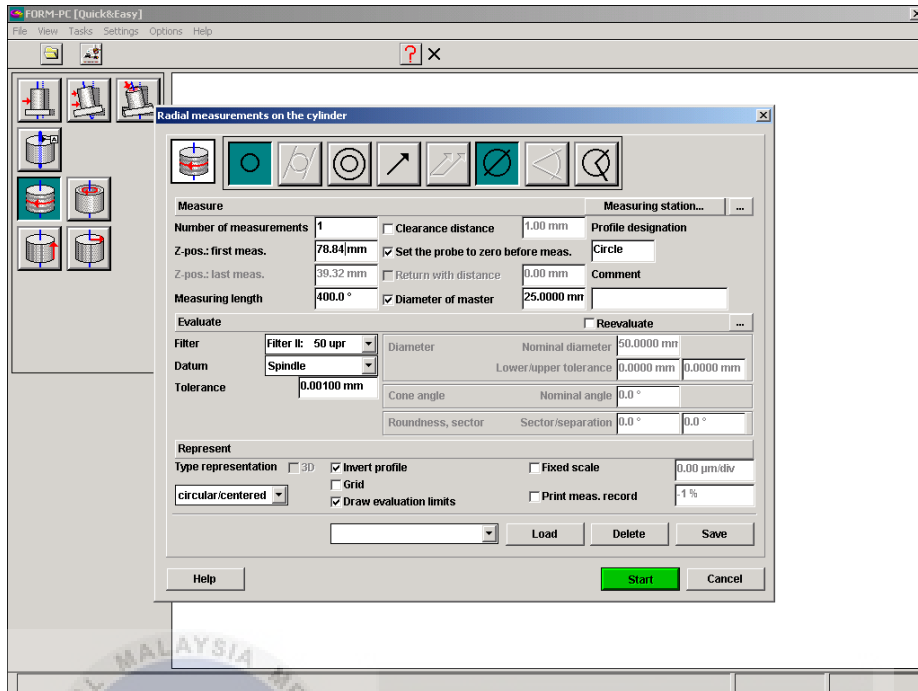
Figure 3.21: Z-axis position of roundness tester
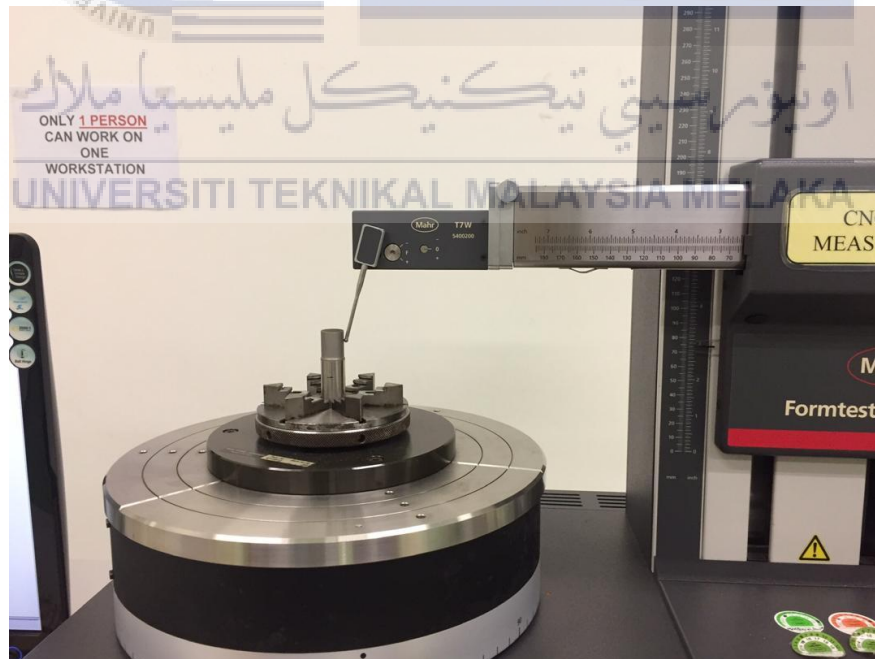
Figure 3.22: CNC Roundness Measuring Machine

3.5.3 Optical Microscope

An optical microscope is a tool used to generate a magnified image of an object specimen. Olympus BX51M reflected light microscope is equipped with UM PLAN FL 5x, 10x, 20x, 50x, and 100x objectives. This microscope from Olympus is designed for looking at materials or metallurgical samples.
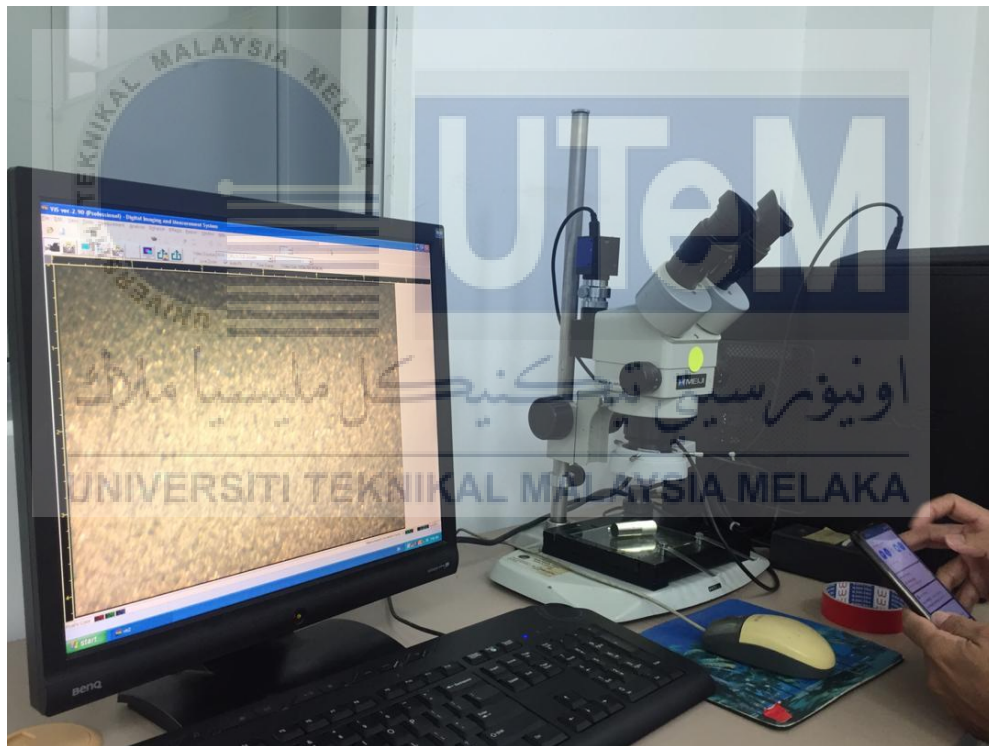
Figure 3.23: Optical microscope

3.5 Data Analysis-ANOVA

Analysis of variance (ANOVA) is the collection of statistical models of the independent groups more than two. There are two types of variables in ANOVA, which is independent and dependent. The Independent variable will be controlled and manipulate by the researcher while the dependent variable is the result of the independent variable. In this project, three-way is used to determine if there is an effect of the AWJT parameter of Inconel 718 alloy productivity and surface roughness.

3.5.1 Procedure of data analysis- Three-way ANOVA

1. Assumption of ANOVA
   a. The population from the sample that will be taken should be approximately normally distributed.
   b. The population from which samples of equal variance (or standard deviation) will be extracted.
   c. The sample of the population must be independent.
   d. The sample size of the group is equal.

2. Hypothesis
   Three sets of the null hypothesis with the two-way ANOVA are:
   a. The population means of the first factor shall be equal.
   b. The population means of the second factor shall be equal.
   c. There is no interaction between the two factors involved.

3. Main effect
   a. Interaction effect (A x B)

i. The interaction effect is the effect of one factor has another factor, and the degree of freedom is the product of two degrees of freedom of each factor.

b. F-tests (F-ratio)

   i. F-test is the mean square for each main effect and the interaction effect divided by the within variance.

4. Three-way ANOVA table

   Table 3.11 shows the data analysis by using two-way ANOVA. The factor of A is the main effect A and B are the main effects of B. The degree of freedom for the main effect A is $I\text{-}1$, the main effect B is $J\text{-}1$, and the main effect C is $K\text{-}1$ where I, K, and J are the group of each factor. N is the total sample size.

Table 3.11: Three-way ANOVA table

Sources	Degrees of Freedom (DF)	Sum of squares (SS)	Mean Square (MS)	F ratio	p-value
A	I-1	SS_A	MS_A	MS_A/MS_E	
B	J-1	SS_B	MS_B	MS_B/MS_E	
C	K-1	SS_C	MS_C	MS_C/MS_E	
A x B	(I-1)(J-1)	SS_{AB}	MS_{AB}	MS_{AB}/MS_E	
A x C	(I-1)(K-1)	SS_{AC}	MS_{AC}	MS_{AC}/MS_E	
C x B	(K-1)(J-1)	SS_{BC}	MS_{BC}	MS_{BC}/MS_E	
Error	N-IJK	SS_E	MS_E		
Total	N-1	SS_T			

5. Interpret the results.

3.5.2 Analysis of three-way ANOVA

Table 3.12 shows the data analysis using three-way ANOVA of three different sources: depth of cut, rotational speed, and nozzle feed rate.

Table 3.12: Analysis of three-way ANOVA

Sources	Degrees of Freedom (DF)	Sum of squares (SS)	Mean Square (MS)	F ratio	p-value
DOC, A					
Feed rate, B					
Rotational speed, c					
A x B					
A x C					
C x B					
Error					
Total					

CHAPTER 4

RESULT AND DISCUSSION

4.1   Results and Discussion

Table 4.1 shows the result of a new coordinate for the x-axis, y-axis, and z-axis by using the formula in (4). The y-axis and z-axis for DOC= 0.1 mm and DOC= 0.3 mm are different due to the stand-off distance being fixed at 8 mm.

Table 4.1: Result of the new coordinate for the position of the x-axis, y-axis, and z-axis

DOC	New Position	New Value
0.1	x_1	67.529
	y_2	213.657
	z_2	115.014
0.3	x_1	67.529
	y_3	213.857
	z_3	113.565

Three testings have been done, which are surface roughness testing, roundness testing, and eccentricity testing. Eight specimens must carry out to achieve the best combination of parameters. All data collected has been recorded in the Design-Expert program, which will

produce an overview and graphics of the results recorded. All experimental findings are listed briefly in this chapter concerning the reported data.
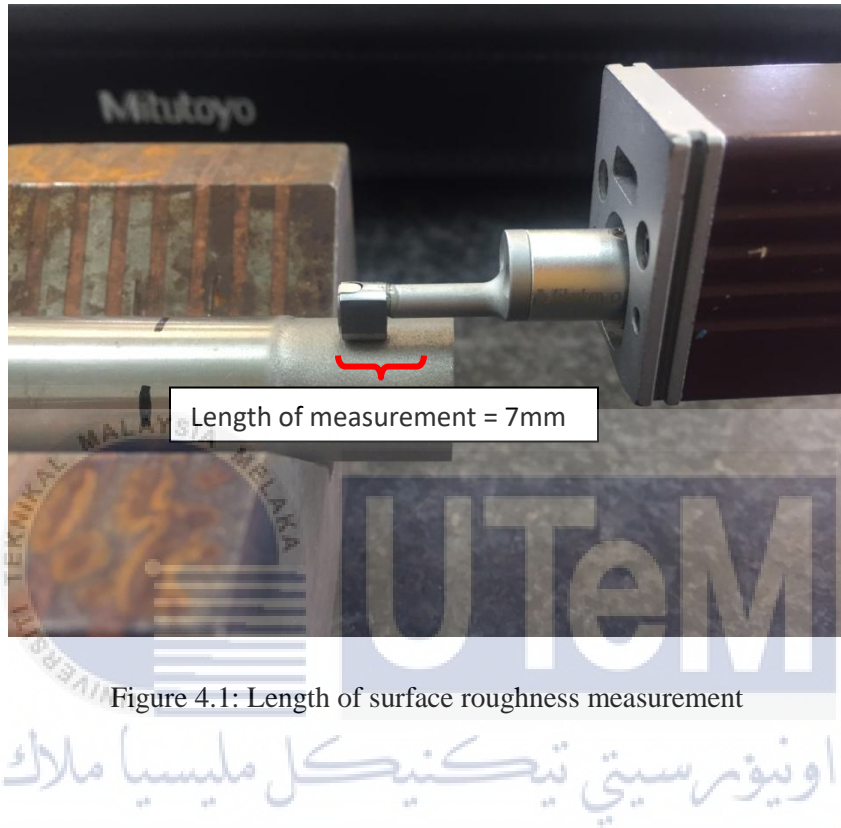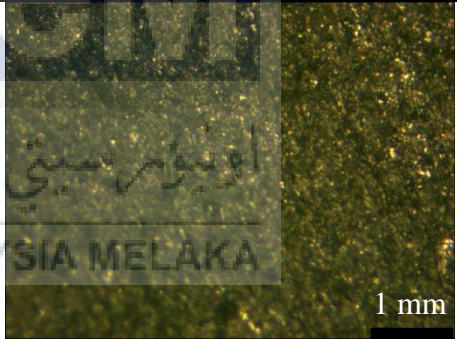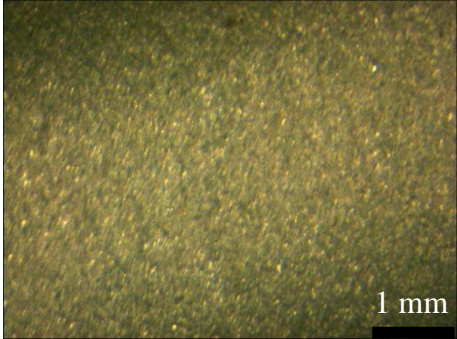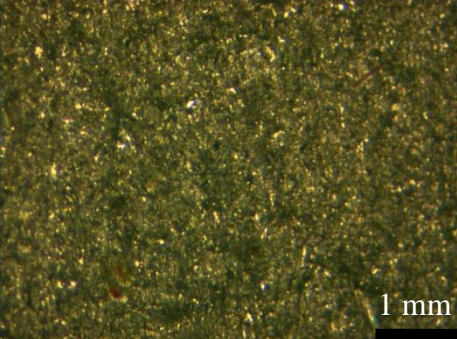
Figure 4.1: Length of surface roughness measurement

The surface roughness tester is conducted with the length of testing is 7 mm, according to ISO-JIS1994 GAUSS (Figure 4.1). Table 4.2 shows the result obtained from the surface roughness testing for eight specimens. Five reading covering five random different spots is obtained for each specimen before getting the average reading. Regarding the results, the lowest reading of surface roughness is 3.792 µm, which is specimen 5 that has the variable of DOC= 0.1 mm, feed rate= 1 mm/min, and rotational speed= 60 rpm. For the highest reading is specimen 3 with DOC= 0.3 mm, feed rate= 1 mm/min and rotational speed= 60 rpm. The diagram of maximum and minimum value for surface roughness is obtained by using the microscope shown in Table 4.3. Regarding Table 4.3, the differences are not significant due to the shape of the specimen is cylindrical and the difference value between the maximum value and minimum value is quite small. Furthermore, no feed mark appears on the specimen after finished machining at the highest variable of feed rate, which is 3 mm/min (Figure 4.2).

Table 4.2: Experimental result from surface roughness testing

Run	DOC, ap (mm)	Feed rate, f (mm/min)	Rotational speed, N (rpm)	Roughness, Ra (µm)					
				1	2	3	4	5	Average
1	0.3	1	90	3.850	3.920	4.980	3.790	3.890	4.086
2	0.1	3	60	4.430	3.910	4.070	5.150	4.010	4.314
3	0.3	1	60	4.400	4.890	4.370	4.580	4.280	4.504
4	0.1	1	90	4.100	4.090	4.200	3.930	3.690	4.002
5	0.1	1	60	3.760	3.330	3.860	3.490	4.520	3.792
6	0.3	3	90	3.920	4.210	4.380	4.360	3.570	4.088
7	0.1	3	90	4.210	3.740	4.090	4.540	4.480	4.212
8	0.3	3	60	4.660	4.230	4.000	4.210	3.880	4.196

Table 4.3: The results of surface roughness picture by using the optical microscope

Surface Roughness	Scope 1x	Scope 4x
Minimum value (Specimen 5; DOC= 0.1 mm, feed rate= 1 mm/min, rotational speed= 60 rpm)	1 mm	1 mm
Maximum value (Specimen 3 DOC= 0.3 mm, feed rate= 1 mm/min, rotational speed= 60 rpm)	1 mm	1 mm
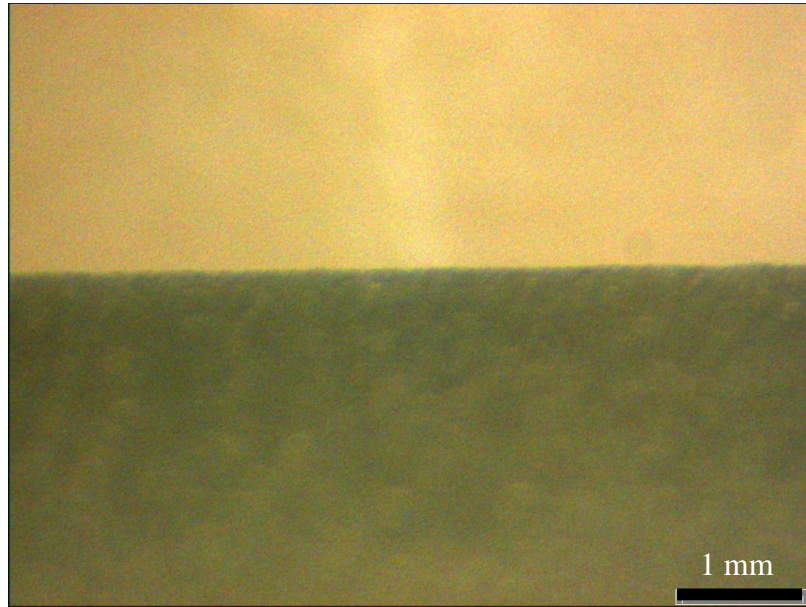
Figure 4.2: No feed mark appear on the specimen at a feed rate of 3 mm/min

Table 4.4 shows the experimental result from average surface roughness testing, roundness testing, eccentricity testing, and percentage of diameter error. The result for roundness testing and eccentricity testing is conducted with the length of testing is 15 mm from the machining surface of specimens while the distance from the table work of the roundness tester is 78 mm. Based on the table, for roundness testing, the minimum value obtained is 1.090 μm, while the maximum value obtained is 1.820 μm. For the eccentricity testing, the lowest value for eccentricity is 0.01 μm while the highest value is 0.05 μm. The value of 0.001 mm is the lowest percentage in the diameter error which is specimen 2 (DOC= 0.1 mm, Feed rate = 3 mm/min, and Rotational speed= 60 rpm) and specimen 6 (DOC= 0.3 mm, Feed rate = 3 mm/min, and Rotational speed= 90 rpm).

65
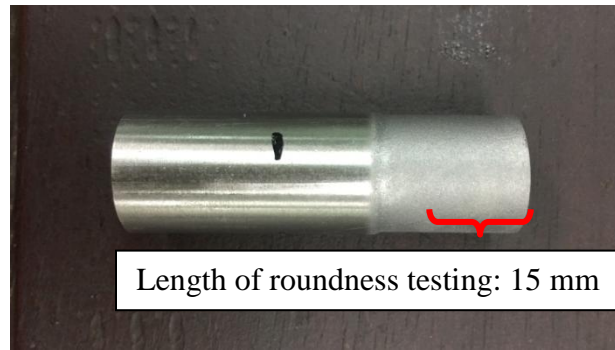
Figure 4.3: Length of roundness testing from the machining surface of the specimen

Table 4.4: The experimental result from average surface roughness testing, roundness testing, eccentricity testing, and percentage of diameter error

Run	DOC (mm)	Feed rate (mm/min)	Rotational speed (rpm)	Surface roughness (µm)	Roundness (µm)	Eccentricity (µm)	Dimension Error (mm)
1	0.3	1	90	4.086	1.460	0.010	0.013
2	0.1	3	60	4.314	1.090	0.010	0.001
3	0.3	1	60	4.504	1.360	0.010	0.012
4	0.1	1	90	4.002	1.590	0.050	0.010
5	0.1	1	60	3.792	1.610	0.020	0.008
6	0.3	3	90	4.088	1.820	0.010	0.001
7	0.1	3	90	4.212	1.530	0.020	0.002
8	0.3	3	60	4.196	1.310	0.030	0.003

Regarding this study's objective, the smoother surface roughness should select the lowest value from the result of surface roughness testing. The best combination variable to obtain smoother surface roughness is DOC of 0.1 mm, the feed rate of 1 mm/min, and the rotational speed at 60 rpm. Meanwhile, for roundness testing, the lowest value is 1.360 µm, while the majority results for eccentricity is 0.01 µm. The result of the value obtained in roundness testing and eccentricity testing is significantly related to each other. So, it is not significant to choose the best combination parameter, which gives the least considerable

response. Based on Figure 4.4, the roundness testing was run on a roundness measuring machine from brand Mahr. The minimum results obtained from roundness testing, as shown in Figure 4.4. All the result for each specimen is attached in Appendices A.
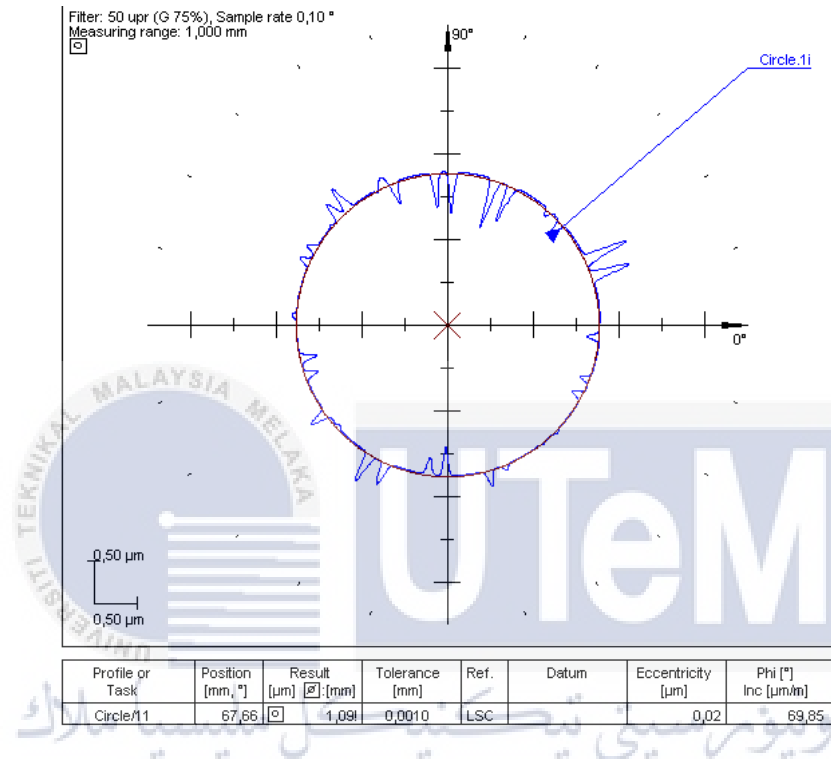
Figure 4.4: The results of roundness testing and eccentricity testing for specimen no 2 (DOC= 0.1 mm, Feed rate = 3 mm/min, and Rotational speed= 60 rpm).

4.2 Analysis Parameter By Using ANOVA

4.2.1 Analysis of parameter effect on surface roughness

The ANOVA results in Table 4.5 show that the "Model F-value" of 364.51 implies the model is significant. There is only 4.01% probability that such a large "Model F-value" will

occur due to noise. The value of "Prob > F" less than 0.05 imply that the model term is significant. In this case, A, B, C, AC, and BC are significant model terms. The value of "Prob >F" higher than 0.10 show the model terms are not significant. The model reduction can improve the model if there are many insignificant model terms (not counting those required to support hierarchy. Based on Table 4.6, the prediction R-Squared of 0.9708 is in reasonable agreement with the adjusted R-squared of 0.9968. Adeq Precision is used to measure the signal to noise ratio. The value of the ratio is greater than 4 is desirable. In these cases, the ratio is 63.320 that indicates an adequate signal. In conclusion, this model can be used to navigate the design space.

Table 4.5: The results of ANOVA for surface roughness

Sources	Sum of squares (SS)	Degrees of Freedom (DF)	Mean Square (MS)	F value	Prob>F	
Model	0.320	6	0.053	364.51	0.0401	Significant
A	0.130	1	0.130	875.46	0.0215	Significant
B	0.043	1	0.043	297.06	0.0369	Significant
C	0.025	1	0.025	175.17	0.0480	Significant
AB	0.023	1	0.023	156.99	0.0507	Relatively significant
AC	0.048	1	0.048	334.67	0.0348	Significant
BC	0.050	1	0.050	347.71	0.0341	Significant
Residual	1.445×10^{-4}	1	1.445×10^{-4}			
Total	0.320	7				

Table 4.6: Data analysis for surface roughness (R-Squared)

Information	Value
Std. dev.	0.012
Mean	4.15
C.V.	0.29
PRESS	9.248×10^{-3}
R-Squared	0.9995
Adj R-Squared	0.9968
Pred R- Squared	0.9708
Adeq Precision	63.320

4.2.2 Analysis of parameter effect on roundness error

The ANOVA results in Table 4.7 show that the "Model F-value" of 10.98 implies the model is significant. There is only 2.12% probability that such a large "Model F-value" will occur due to noise. The value of "Prob > F" less than 0.05 imply that the model term is significant. In this case, A is significant model terms. The value of "Prob >F" higher than 0.10 show the model terms are not significant. The model reduction can improve the model if there are many insignificant model terms (not counting those required to support hierarchy. Based on Table 4.8, shows that the value of prediction R-Squared is 0.5670 which is not close to the adjusted R-Squared of 0.8106 as one might normally expect. This may indicate a large block effect or a possible problem with the model and data. So, it needs to consider response transformation, cook's distance, and normal probability. For the adeq precision, it is greater than 4 which is 9.147 that indicates an adequate signal. As a conclusion, this model can be used to navigate the design space.

Table 4.7: The results of ANOVA for roundness

Sources	Sum of squares (SS)	Degrees of Freedom (DF)	Mean Square (MS)	F value	Prob>F	
Model	0.310	3	0.010	10.98	0.0212	Significant
A	0.220	1	0.220	23.87	0.0081	Significant
B	0.041	1	0.041	4.38	0.1044	Not significant
C	0.044	1	0.044	4.70	0.0961	Not significant
Residual	0.037	4	9.263×10^{-3}			
Total	0.340	7				

Table 4.8: Data analysis for roundness (R-Squared)

Information	Value
Std. dev.	0.096
Mean	1.47
C.V.	6.54
PRESS	0.15
R-Squared	0.8918
Adj R-Squared	0.8106
Pred R- Squared	0.5670
Adeq Precision	9.147

69

4.2.3 Analysis of parameter effect on eccentricity error

The ANOVA results in Table 4.9 show that the "Model F-value" of 9.75 implies the model is significant. There is only 4.57% probability that such a large "Model F-value" will occur due to noise. The value of "Prob > F" less than 0.05 imply that the model term is significant. In this case, B and BC are significant model terms. The value of "Prob >F" higher than 0.10 show the model terms are not significant. The model reduction can improve the model if there are many insignificant model terms (not counting those required to support hierarchy. Based on Table 4.10, shows that the value of prediction R-Squared is 0.4921 which is not close to the adjusted R-Squared of 0.8333 as one might normally expect. This may indicate a large block effect or a possible problem with the model and data. So, it needs to consider response transformation, cook's distance, and normal probability. For the adeq precision, it is greater than 4 which is 8.764 that indicates an adequate signal. In conclusion, this model can be used to navigate the design space.

Table 4.9: The results of ANOVA for eccentricity

Sources	Sum of squares (SS)	Degrees of Freedom (DF)	Mean Square (MS)	F value	Prob>F	
Model	1.300×10^{-3}	4	3.250×10^{-4}	9.75	0.0457	Significant
A	2.000×10^{-4}	1	2.000×10^{-4}	6.00	0.0917	Not significant
B	4.500×10^{-4}	1	4.500×10^{-4}	13.50	0.0349	Significant
C	2.000×10^{-4}	1	2.000×10^{-4}	6.00	0.0917	Not significant
BC	4.500×10^{-4}	1	4.500×10^{-4}	13.50	0.0349	Significant
Residual	1.000×10^{-4}	3	3.333×10^{-5}			
Total	1.400×10^{-4}	7				

Table 4.10: Data analysis for eccentricity (R-Squared)

Information	Value
Std. dev.	5.774×10^{-3}
Mean	0.020
C.V.	28.87
PRESS	7.111×10^{-4}
R-Squared	0.9286
Adj R-Squared	0.8333
Pred R- Squared	0.4921
Adeq Precision	8.764

4.2.4 Analysis of parameter effect on diameter error

The ANOVA results in table 4.11 show that the "Model F-value" of 27.35implies the model is significant. There is only 1.07% probability that such a large "Model F-value" will occur due to noise. The value of "Prob > F" less than 0.05 imply that the model term is significant. In this case, AB is significant model terms. The value of "Prob >F" higher than 0.10 show the model terms are not significant. The model reduction can improve the model if there are many insignificant model terms (not counting those required to support hierarchy. Based on table 4.12, the prediction R-Squared of 0.8102 is in reasonable agreement with the adjusted R-squared of 0.9377. Adeq Precision is used to measure the signal to noise ratio. The value of the ratio is greater than 4 is desirable. In these cases, the ratio is 12.272 that indicates an adequate signal. In conclusion, this model can be used to navigate the design space.

71

Table 4.11: The results of ANOVA for the percentage of diameter error

Sources	Sum of squares (SS)	Degrees of Freedom (DF)	Mean Square (MS)	F value	Prob>F	
Model	1.776×10^{-4}	4	4.441×10^{-5}	27.35	0.0107	Significant
A	8.581×10^{-6}	1	8.581×10^{-6}	5.28	0.1051	Not significant
B	3.951×10^{-6}	1	3.951×10^{-6}	2.43	0.2167	Not significant
C	3.373×10^{-6}	1	3.373×10^{-6}	2.08	0.2451	Not significant
AB	1.617×10^{-4}	1	1.617×10^{-4}	99.60	0.0021	Significant
Residual	4.871×10^{-6}	3	1.624×10^{-6}			
Total	1.825×10^{-4}	7				

Table 4.12: Data analysis for the percentage of diameter error (R-Squared)

Information	Value
Std. dev.	1.274×10^{-3}
Mean	6.103×10^{-3}
C.V.	20.88
PRESS	3.464×10^{-5}
R-Squared	0.9733
Adj R-Squared	0.9377
Pred R- Squared	0.8102
Adeq Precision	12.272

4.3   Model development in terms of Actual Factors

The data need to be measured and legitimate the experiment by scientific prediction model that develops by utilizing ANOVA. The calculation is to verify whether the experiment has a huge contrast compared to the model.

a) Mathematical model development for surface roughness

The surface roughness, Ra can be expressed by:

Ra $= + 2.4830 + (3.6950 \text{ ap}) + (0.4295 \text{ f}) + (0.0247 \text{ N}) - (0.5325 \text{ ap} \cdot \text{f}) - (0.0518 \text{ ap} \cdot \text{N}) - (5.2833 \times 10^{-3} \text{ f} \cdot \text{N})$

Where, ap $= $ Depth of Cut (DOC)

f $= $ Feed rate

N $= $ Rotational speed

b) Mathematical model development for roundness

The roundness, R of the sample can denoted by:

R $= - 1.6500 + (1.6625 \text{ ap}) - (0.0713 \text{ f}) - (4.9166 \times 10^{-3} \text{ N})$

Where, ap $= $ Depth of Cut (DOC)

f $= $ Feed rate

N $= $ Rotational speed

c) Mathematical model development for eccentricity

The eccentricity, e of the sample can be calculated by:

e $= - 0.0550 + (0.0500 \text{ ap}) + (0.0450 \text{ f}) + (6.6670 \times 10^{-4} \text{ N}) - (5.0000 \times 10^{-4} \text{ f} \cdot \text{N})$

Where, ap $= $ Depth of Cut (DOC)

f   = Feed rate

N   = Rotational speed

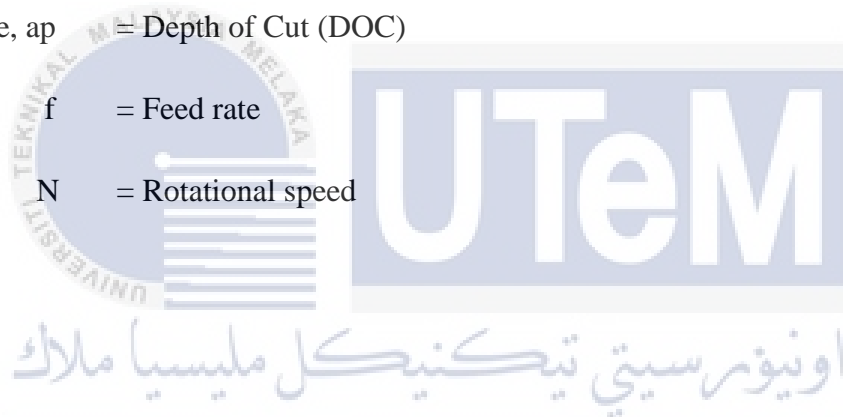**d) Mathematical model development for diameter error**

The diameter error, dim_e can be calculated by:

Dim_e = + 0.0308 - (0.1003 ap) - (9.69505×10^{-3} f) - (4.3290×10^{-5} N) + (0.0450 ap · f)

Where, ap   = Depth of Cut (DOC)

f   = Feed rate

N   = Rotational speed

4.4   Comparison Between Model And Experiment

The comparison is made by taking all response which is surface roughness, roundness, eccentricity and diameter error in the experiment

4.4.1   The diagnostic plot for surface roughness

In Figure 4.5, it shows the normal plot of residual in a straight line and all of the point is balanced. The tendency for the position of the point change is slight because it has a less average error. Figure 4.6 indicates the effect of the model for each movement in the cook's

distance. It shows that all the specimens have a constant value for the cook's distance which is 1.010. Figure 4.7 reveals the box-cox plot which determines the most appropriate power transformation in order to apply into the roughness. The current lambda is 1 while the best value pf lambda is 2.4. The recommend transform is power transformation.
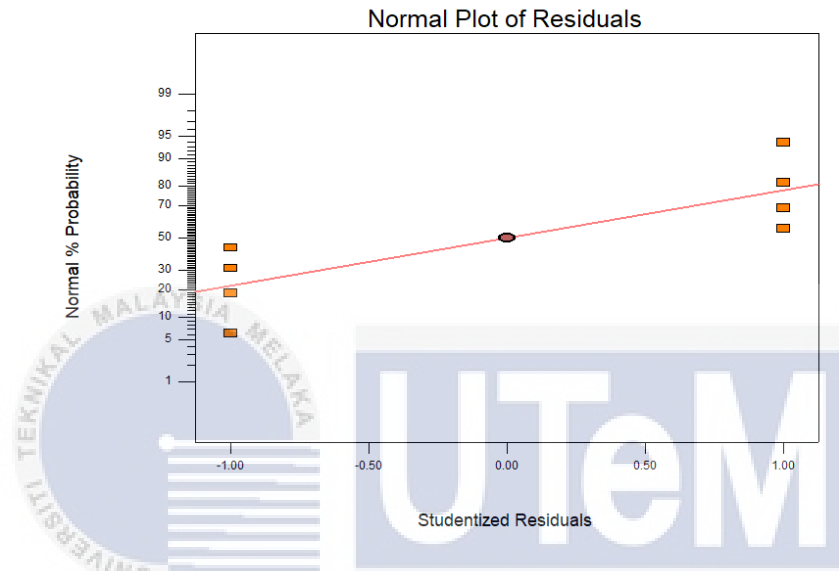

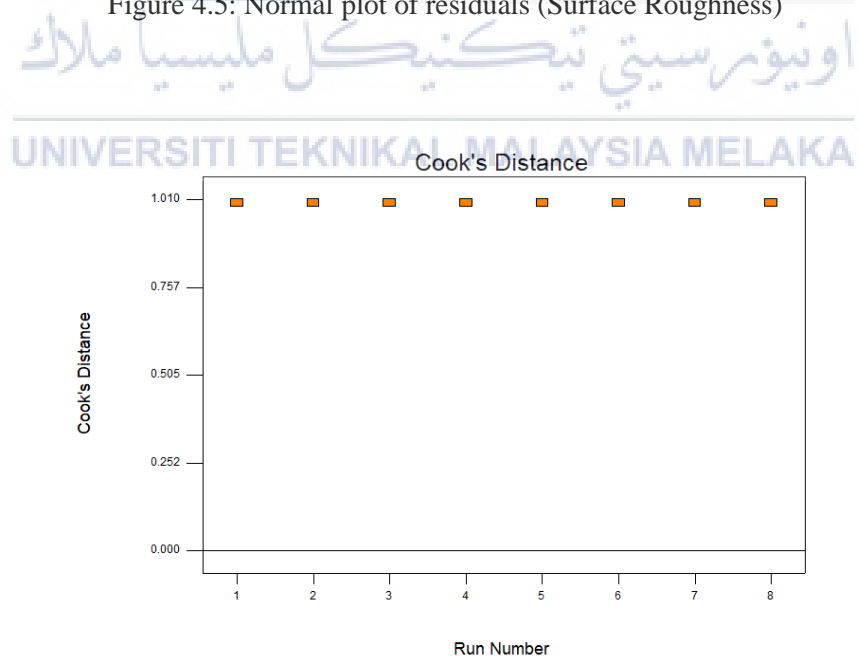Figure 4.5: Normal plot of residuals (Surface Roughness)

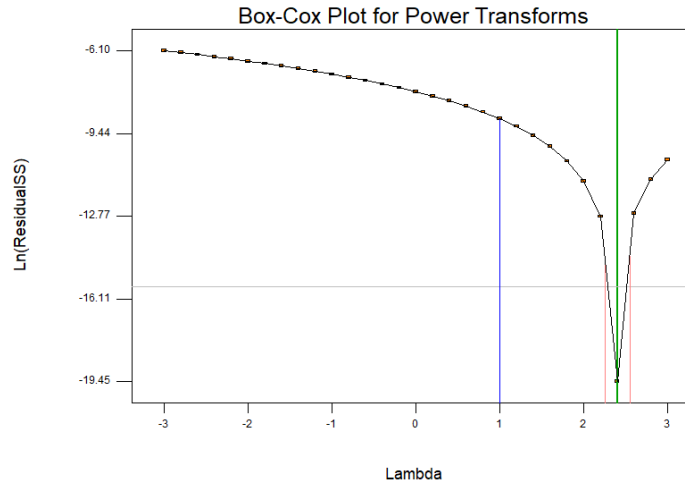Figure 4.6: Cook's distance (Surface Roughness)

Figure 4.7: Box-cox plot for power transforms (Surface Roughness)

4.4.2 The diagnostic plot for roundness

In Figure 4.8, shows the normal plot of residual in a straight line, and all of the points are closed. The tendency for the position of the point change is slight because it has a less average error. Figure 4.9 indicates the effect of the model for each movement in the cook's distance. Two points have a higher value that exceeds more than 0.5 probability value while the others remain in a range which is below 0.5. Figure 4.10 reveals the box-cox plot which determines the most appropriate power transformation in order to apply into the roundness. The current lambda is 1 while the best value of lambda is 1.38. There is no recommend transform so the value of lambda will remain 1.
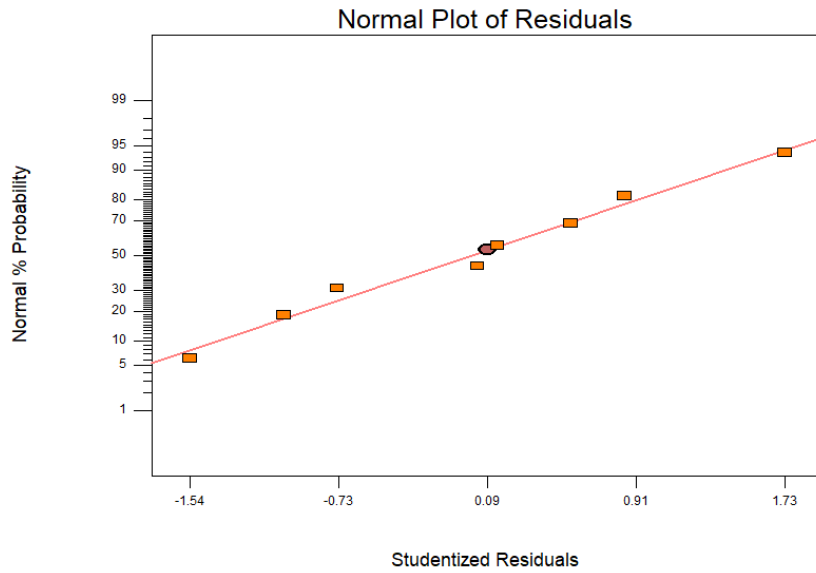
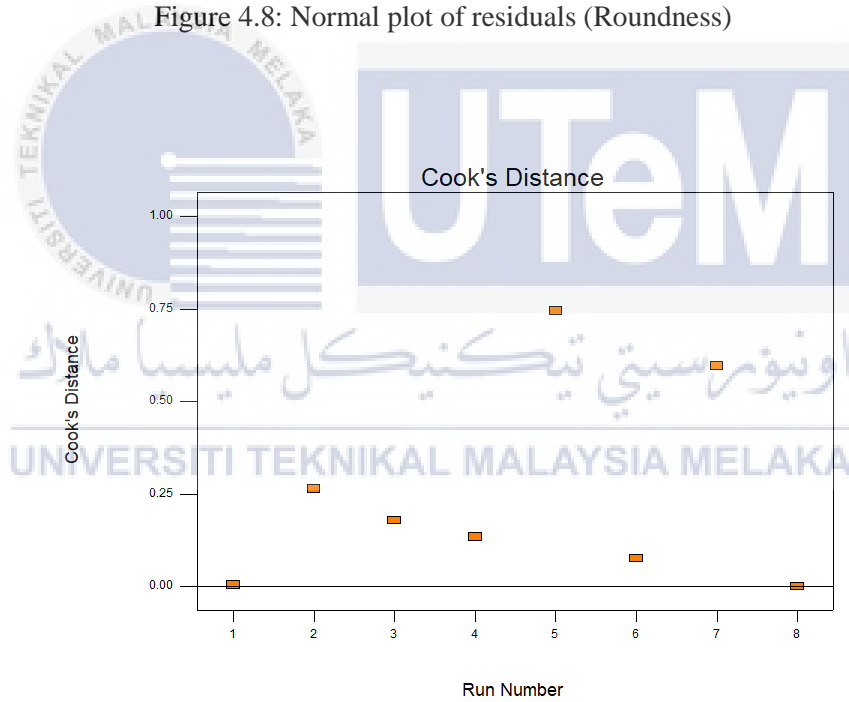Figure 4.8: Normal plot of residuals (Roundness)

Figure 4.9: Cook's distance (Roundness)

DESIGN-EXPERT Plot
Roundness

Lambda
Current = 1
Best = 1.38
Low C.I. = -2.3
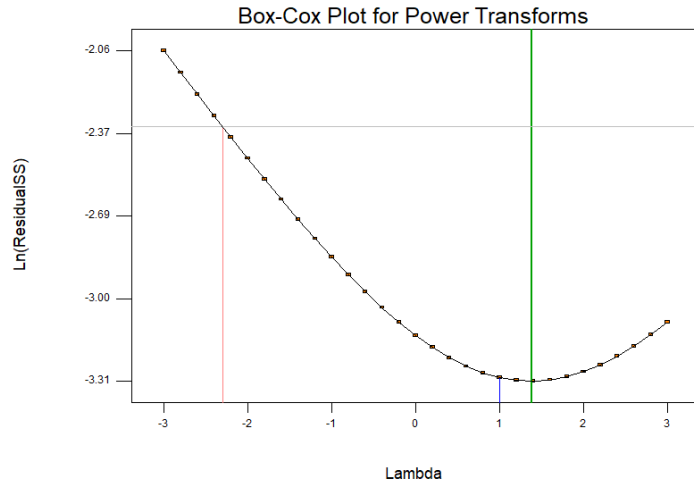High C.I. = 5.01

Recommend transform:
None
 (Lambda = 1)

Box-Cox Plot for Power Transforms

Figure 4.10: Box-cox plot for power transforms (Roundness)

4.4.3   The diagnostic plot for eccentricity

In Figure 4.11, shows the normal plot of residual in a straight line, and all of the points are balanced. The tendency for the position of the point change is slight because it has a less average error. Figure 4.12 indicates the effect of the model for each movement in the cook's distance. There are four points that have a constantly higher value which exceeds more than 0.5 probability value while the others have the lowest probability value which is 0.00. Figure 4.13 reveals the box-cox plot which determines the most appropriate power transformation in order to apply into the roundness. The current lambda is 1 while the best value of lambda is 0.12. There is no recommend transform so the value of lambda will remain 1.
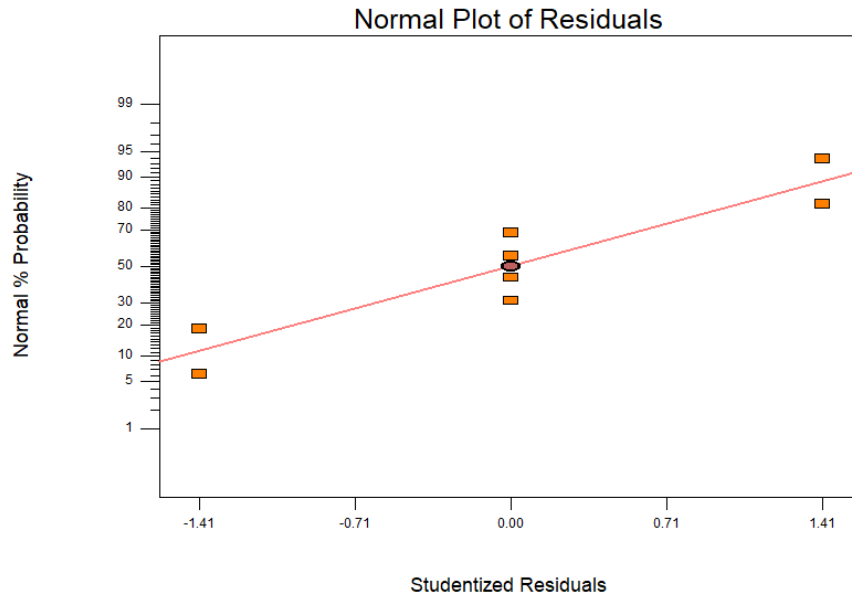
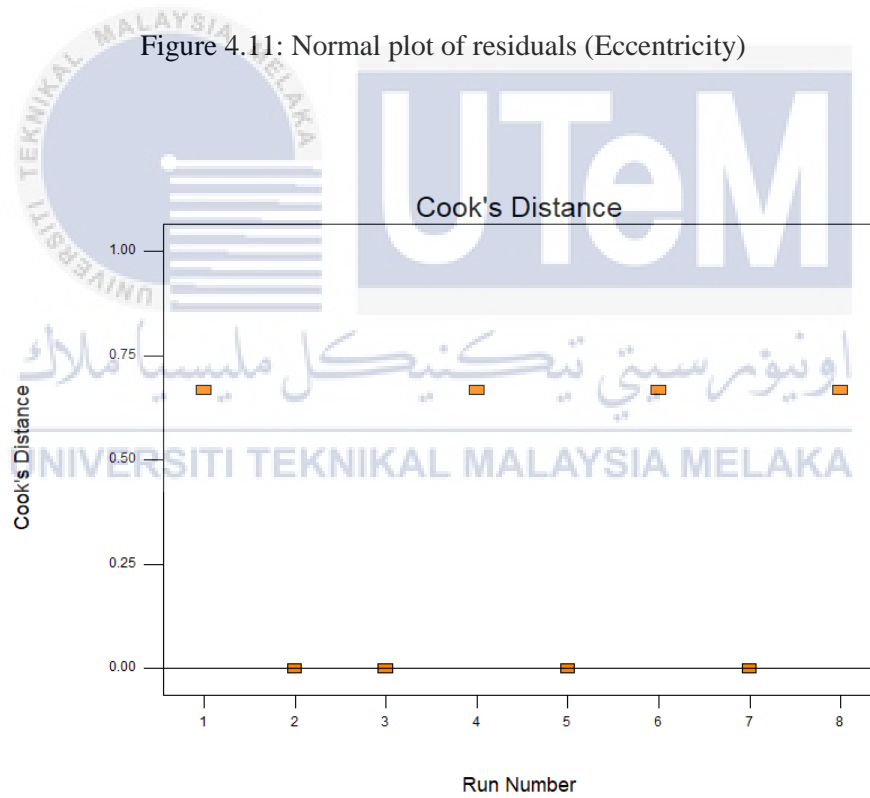Figure 4.11: Normal plot of residuals (Eccentricity)

Figure 4.12: Cook's distance (Eccentricity)

DESIGN-EXPERT Plot
Ecentricity

Lambda
Current = 1
Best = 0.12
Low C.I. = -2.24
High C.I. = 1.25

Recommend transform:
None
 (Lambda = 1)

Box-Cox Plot for Power Transforms

Ln(ResidualSS)

Lambda
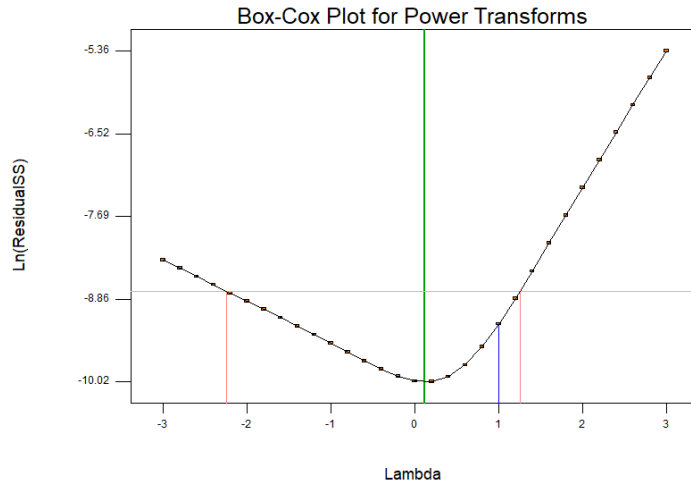
Figure 4.13: Box-cox plot for power transforms (Eccentricity)

4.4.4   The diagnostic plot for diameter error

In Figure 4.14, shows the normal plot of residual in a straight line, and all of the points are closed. The tendency for the position of the point change is slight because it has a less average error. Figure 4.15 indicates the effect of the model for each movement in the cook's distance. Two points have a higher value that exceeds more than 0.5 probability value while the others remain in a range which is below 0.5. Figure 4.16 reveals the box-cox plot which determines the most appropriate power transformation in order to apply into the roundness. The current lambda is 1 while the best value of lambda is 1.17. There is no recommend transform so the value of lambda will remain 1.

Figure 4.14: Normal plot of residuals (Diameter Error)
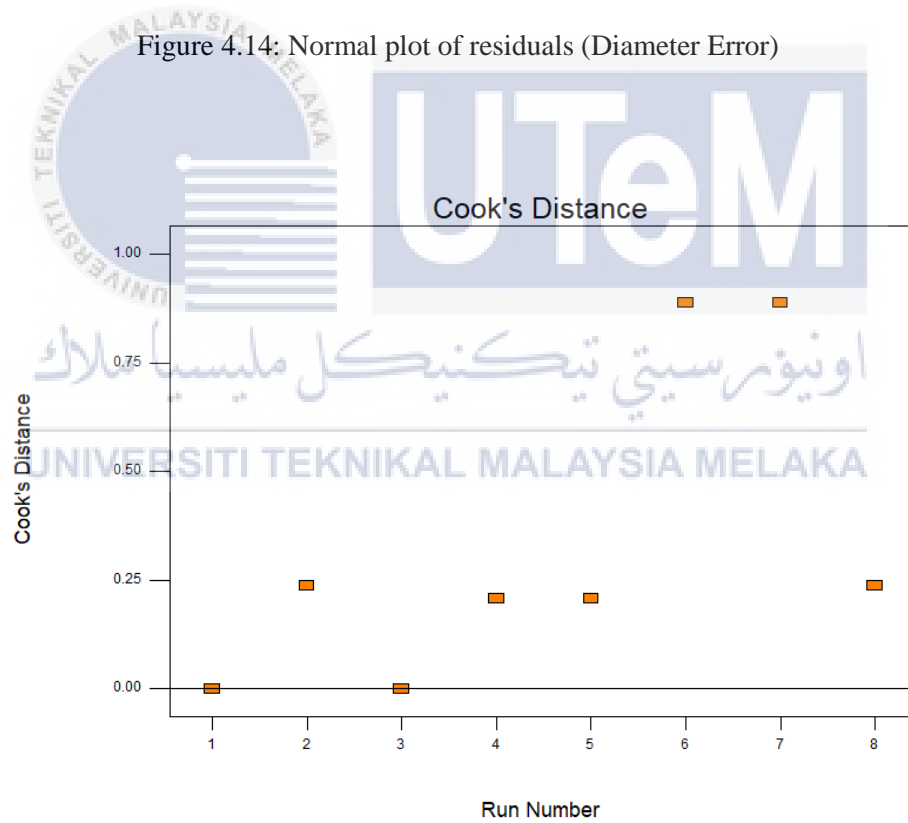
Figure 4.15: Cook's distance (Diameter Error)

81

DESIGN-EXPERT Plot
Diameter error

Lambda
Current = 1
Best = 1.17
Low C.I. = 0.19
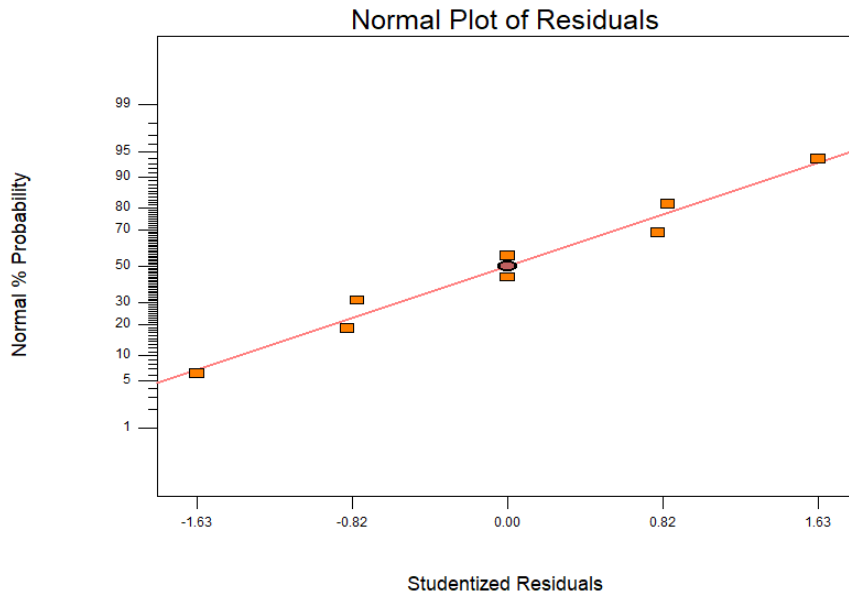High C.I. = 2.11

Recommend transform:
None
(Lambda = 1)
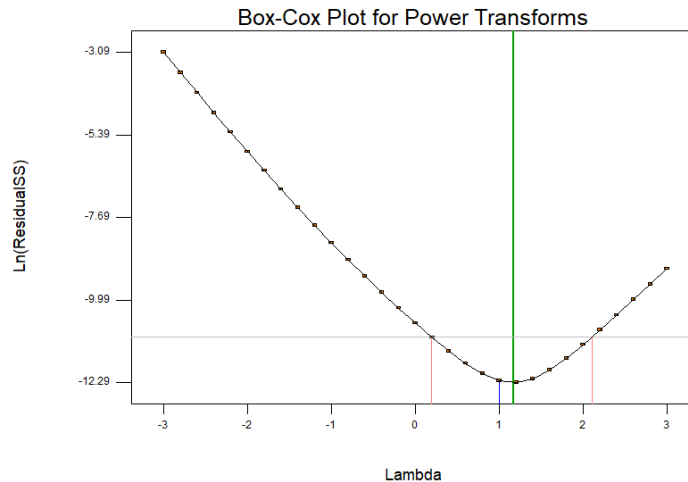
Figure 4.16: Box-cox plot for power transforms (Diameter Error)

4.5 Effect of Parameter Into The Response

4.5.1 Effect of parameters into surface roughness

All the results are generated from ANOVA shows the interaction graph between factors and response. For the surface roughness, there is only an interaction graph that will give a huge influence on the value of surface roughness. The interaction involved the DOC versus feed rate parameter versus rotational speed and feed rate versus rotational speed. Figure 4.17 shows that the surface roughness gives excellent performance when the DOC is 0.3 mm. It more significant when a feed rate of 3mm/min is applied. In feed rate 1mm/min, it shows less effectiveness on the surface roughness especially in 0.1mm of DOC.

DESIGN-EXPERT Plot

Surface Roughness

X = A: DOC
Y = B: Feed Rate

■ B- 1.000
▲ B+ 3.000
Actual Factor
C: Rotational Speed = 75.00
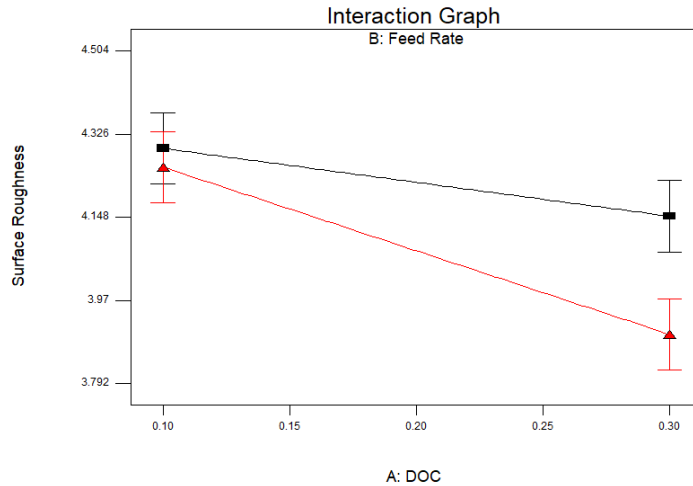
Interaction Graph

Figure 4.17: Interaction graph for surface roughness; DOC vs Feed rate

The integration graph of figure 4.18 shows that the surface roughness is falling to a minimum value that indicates the best value for surface roughness when the DOC is 0.3mm, and rotational speed is 90rpm. When the parameter of rotational speed is 60 rpm is used, it indicates the best value on surface roughness's value when 0.1mm of DOC is applied, but it becomes slightly higher on the result of surface roughness value when DOC is 0.3mm.

DESIGN-EXPERT Plot

Surface Roughness

X = A: DOC
Y = C: Rotational Speed

■ C- 60.000
▲ C+ 90.000
Actual Factor
B: Feed Rate = 2.00
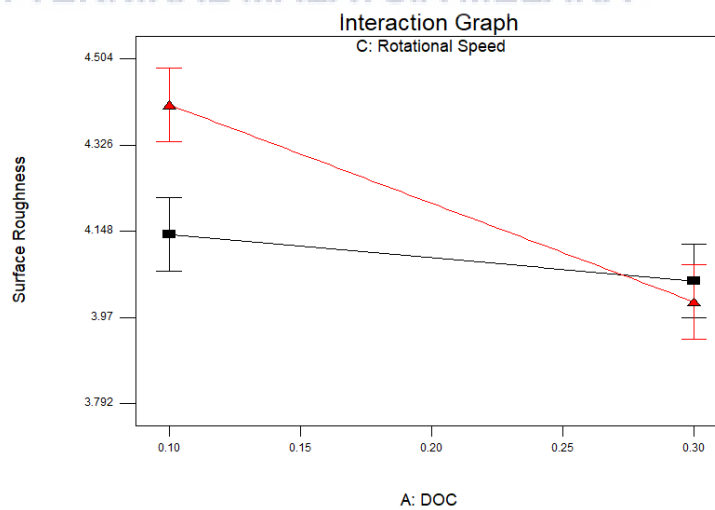
Interaction Graph

Figure 4.18: Interaction graph for surface roughness; DOC vs Rotational Speed

83

The graph in figure 4.19 reveals that the feed rate of 3mm/min shows a considerable impact on specimens' surface roughness with 90rpm of rotational speed. Meanwhile, the slow feed rate of 1mm/min indicates the best surface roughness when the rotational speed at 60rpm. At the rotational speed of 60 rpm, it becomes slightly rough on the surface of a specimen when the feed rate is 3mm/min.
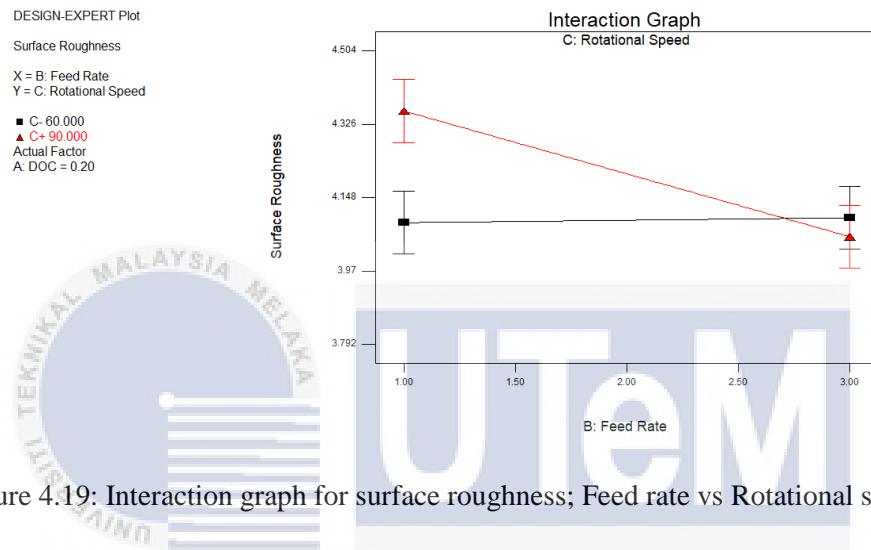
Figure 4.19: Interaction graph for surface roughness; Feed rate vs Rotational speed

4.5.2 Effect of parameters into roundness error

Regarding the one-factor plot graph of Figure 4.20, it shows that the minimum value of roundness is obtained at the DOC equal to 0.1mm. As the DOC is increased to 0.3mm, the roundness value also increased.
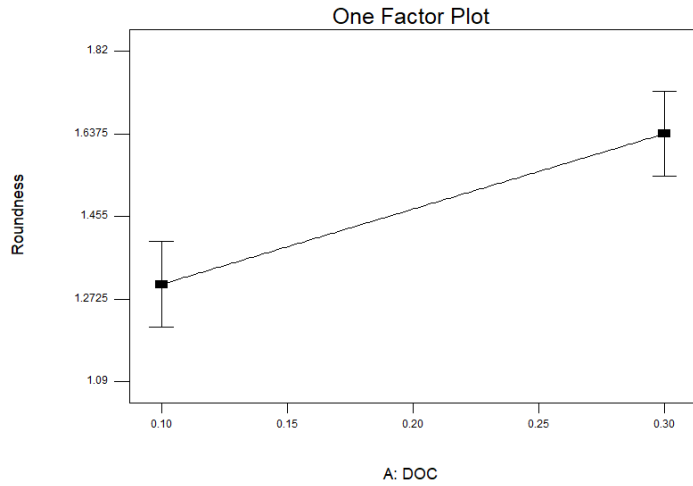
Figure 4.20: One-factor plot graph for roundness; DOC

Figure 4.21 proclaims that the value of roundness decreased when the feed rate is increased. The same pattern is observed in the relationship between roundness and rotational (Figure 4.22), where the increasing value of rotational speed will give excellent results in roundness.
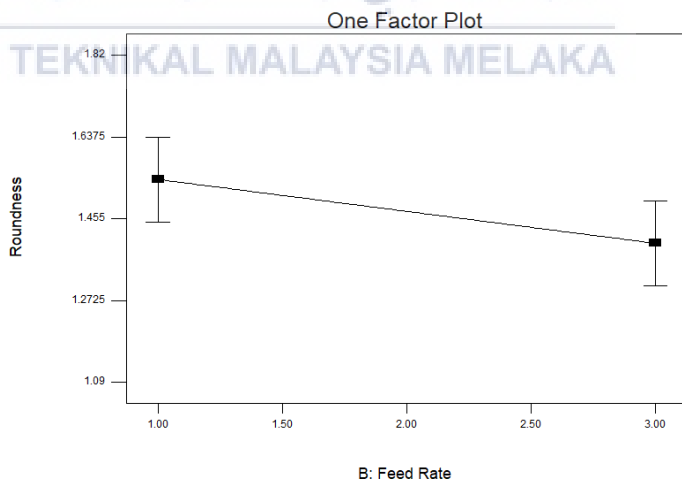
Figure 4.21: One-factor plot a graph for roundness; Feed rate
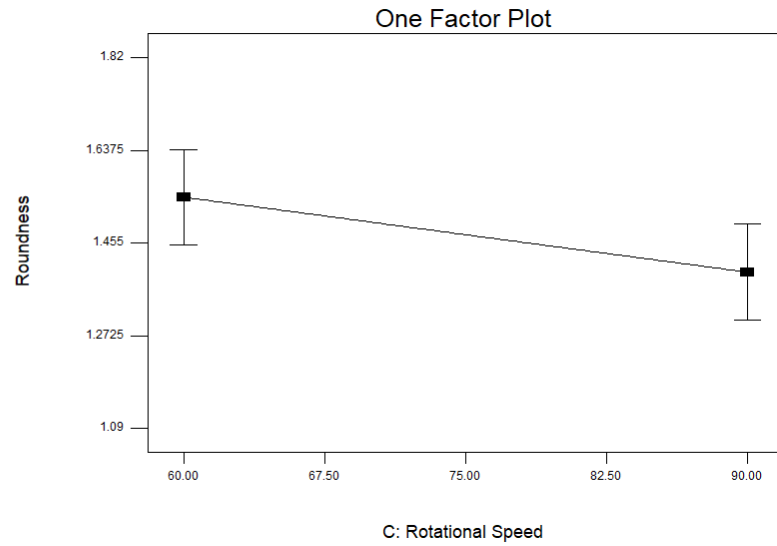
Figure 4.22: One-factor plot graph for roundness; Rotational speed
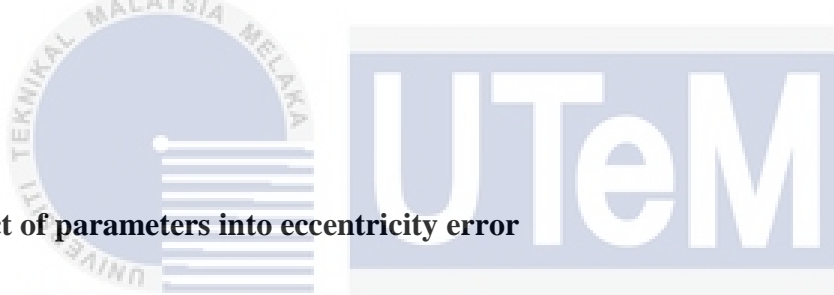
4.5.3 Effect of parameters into eccentricity error

Figure 4.23 indicates a one-factor plot graph for the factor of DOC. It shows that the minimum value of DOC, which 0.1mm shows excellent results for eccentricity. The less effective results of eccentricity can be observed when DOC is increased to 3mm/min.
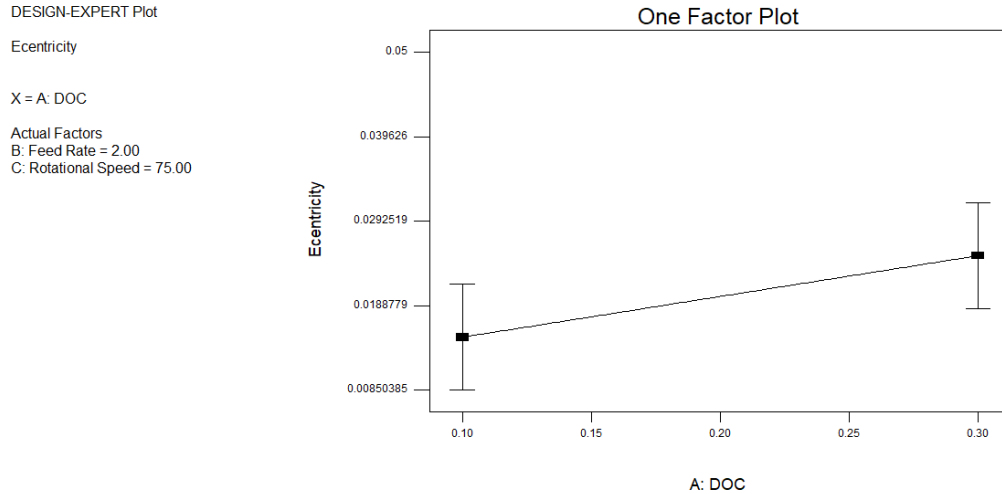
One Factor Plot

Figure 4.23: One-factor plot graph of eccentricity; DOC

The interaction graph for eccentricity in figure 4.24 shows that the more effectiveness of eccentricity's value occurs in the feed rate of 1 mm/min with the rotational speed of 60rpm. Simultaneously, at the same rotational speed, which is 60rpm, it shows that the value of eccentricity is less effective when the value of feed rate is increased to 3 mm/min. Meanwhile, the value of the rotational speed of 90 rpm shows the minimum value of eccentricity when the feed rate of 3 mm/min.

Interaction Graph
C: Rotational Speed
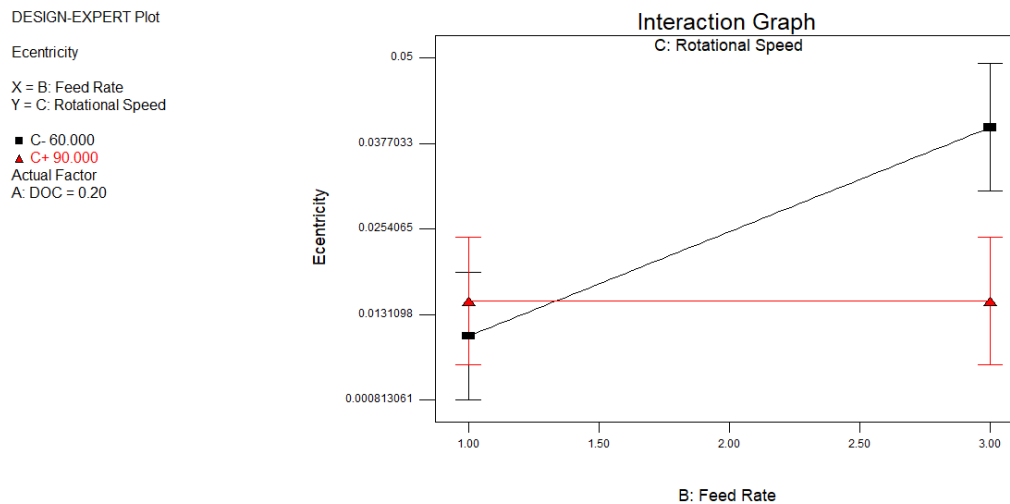
Figure 4.24: Interaction graph for eccentricity; Feed rate vs Rotational speed

87

4.5.4   Effect of parameters into the diameter error

Figure 4.25 reveals that the dimensional error will affect rotational speed where the minimum value of diameter error is obtained when the rotational speed increases during the machining process.
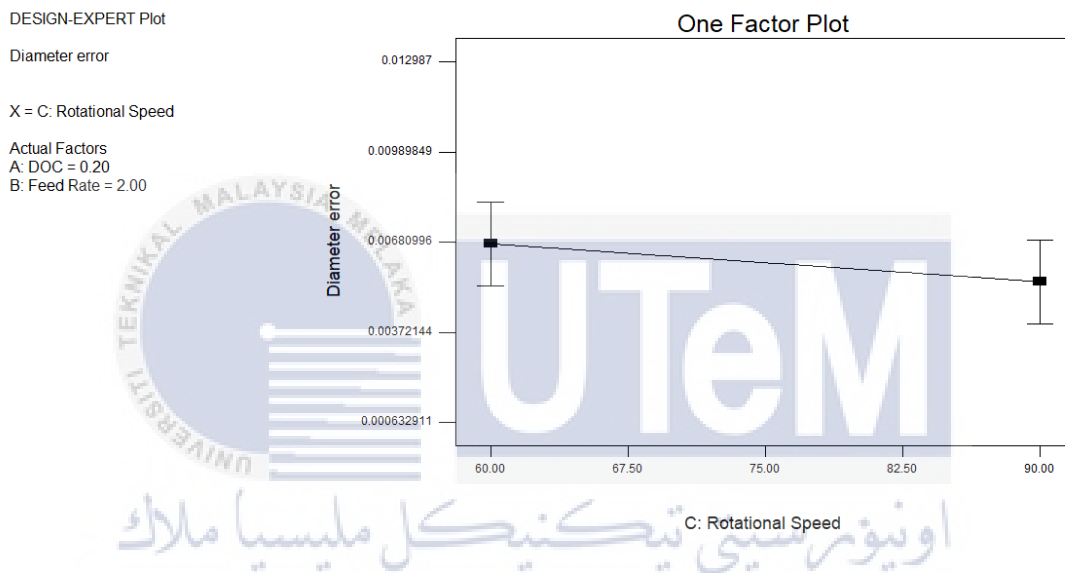
Figure 4.25: One-factor plot graph for dimension error; Rotational speed

Based on Figure 4.26, shows the interaction between factors and response. The interaction graph of DOC versus feed rate shows the diameter error of the specimens is reduced when the DOC is 0.1 mm, and the feed rate is 3 mm/min. The same roundness results can be obtained when the DOC is 0.3 mm, and the feed rate is 1 mm/min.

DESIGN-EXPERT Plot

Diameter error

X = A: DOC
Y = B: Feed Rate

■ B- 1.000
▲ B+ 3.000
Actual Factor
C: Rotational Speed = 75.00
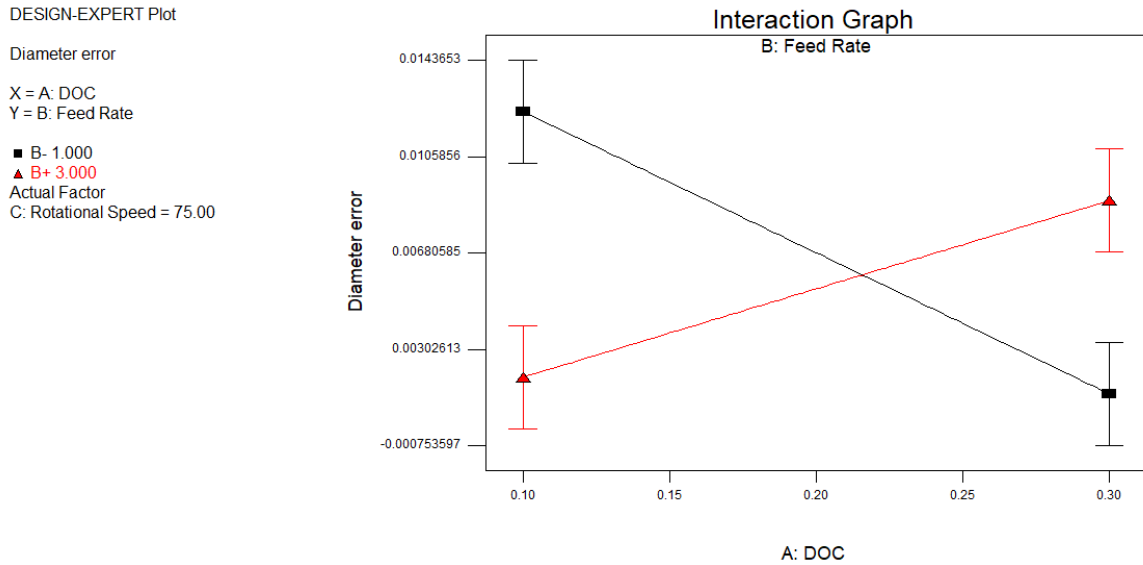
Figure 4.26: Interaction graph for dimension error; DOC vs Feed rate

4.6   Parameter Optimization By Using The Full Factorial Method

Optimizing the parameter is the next step after making ANOVA. The optimized process is assisted by Design-Expert software, and the characteristics target for optimum response is shown in table 4.13. This process's primary goal is to get the minimum target value of surface roughness, roundness, eccentricity, and dimension error. All the parameter is set into the "in range" to generate the ideal respond.

Table 4.13: Characteristic target for optimum responses

Name	Goal	Upper limit	Lower limit
DOC, ap (mm)	In range	0.1	0.3
Feed rate, f (mm/min)	In range	1	3
Rotational speed, N (rpm)	In range	60	90
Surface roughness (μm)	Minimum	3.792	4.504
Roundness (μm)	Minimum	1.090	1.820
Eccentricity (μm)	Minimum	0.010	0.050
Diameter error (mm)	Minimum	0.00063	0.01299

89

4.7   Optimization Of Combination Parameter

Table 4.14 shows the optimum value of surface roughness, roundness, eccentricity, and dimension error response. The ideal solution is no. 1 because the combination of parameters generates the optimum value of the response. All the responses are in optimum value which is a smaller value is observed compared to other results. Besides, the desirability is almost to 1. The ideal combination of the parameter is 0.15mm of DOC, 3mm/min of feed rate, and 90rpm of rotational speed. Figure 4.27 shows the ramps graph for optimum responses which is solution no.1.

Table 4.14: Selection of the optimum combination of parameter

No.	DOC	Feed rate	Rotational speed	Surface roughness	Roundness	Eccentricity	Dimension error	Desirability
1	0.15	3.00	90.00	4.17324	1.2484	0.01266	3.130×10^{-3}	0.721
2	0.15	3.00	90.00	4.16886	1.2512	0.01274	3.189×10^{-3}	0.721
3	0.16	3.00	89.91	4.16626	1.2533	0.01287	3.227×10^{-3}	0.721
4	0.16	2.96	90.00	4.16274	1.2621	0.01298	3.462×10^{-3}	0.715
5	0.11	3.00	90.00	4.28230	1.1778	0.01053	1.661×10^{-3}	0.706
6	0.15	3.00	85.66	4.17402	1.26642	0.01618	3.249×10^{-3}	0.696
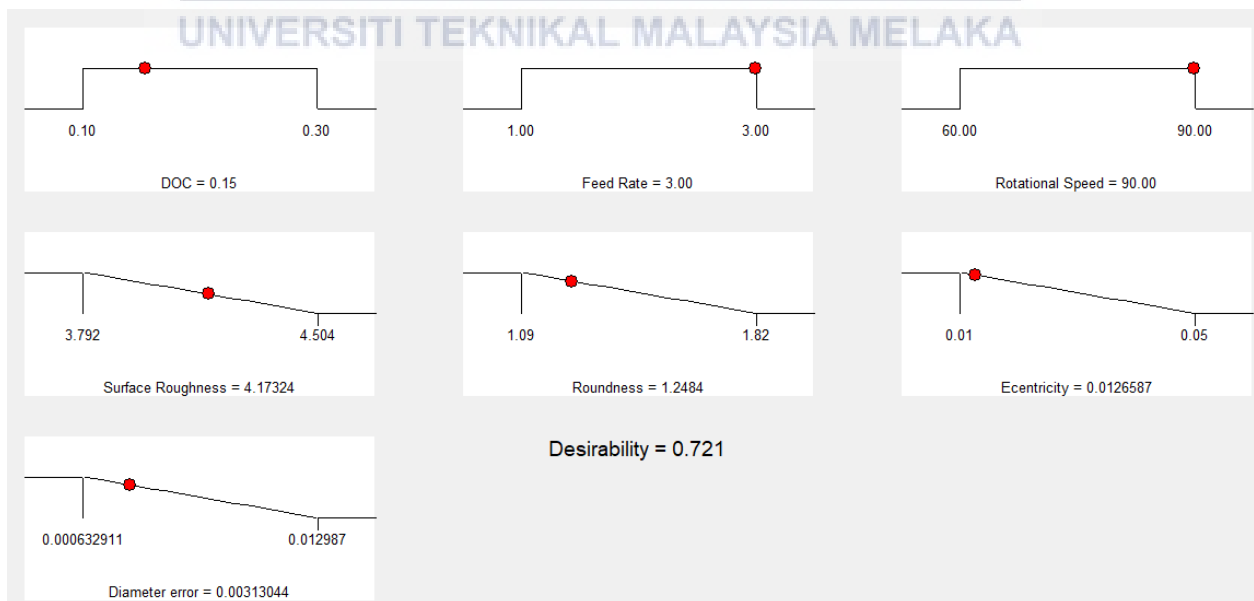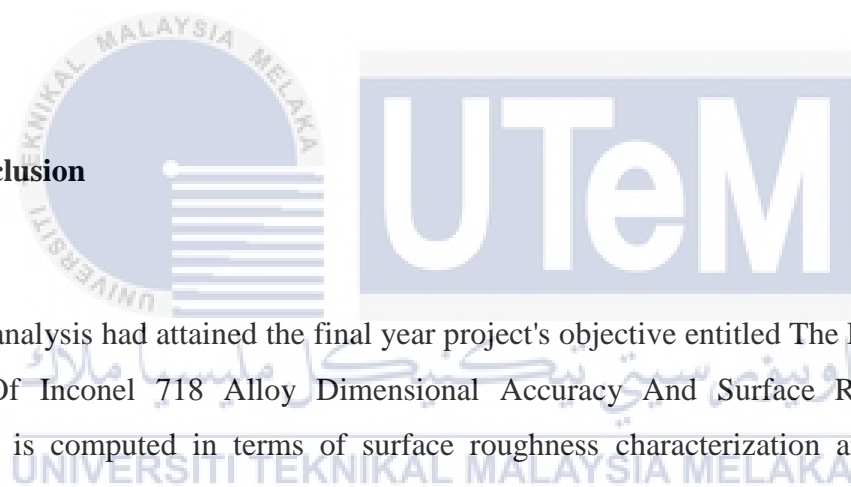
Figure 4.27: Generation of optimum responses from the ideal combination of parameter

90

CHAPTER 5

CONCLUSION AND RECOMMENDATION

5.1   Conclusion

The analysis had attained the final year project's objective entitled The Effect of AWJT Parameter Of Inconel 718 Alloy Dimensional Accuracy And Surface Roughness. The performance is computed in terms of surface roughness characterization and dimensional accuracy, including roundness, eccentricity, and dimension error. The conclusion is as follows:

1. The parameter of DOC found as the most significant factors on surface roughness which is 0.0215 followed by the interaction between feed rate and rotational speed which is 0.0341, the interaction between DOC and rotational speed which is 0.0348, the factor of feed rate which is 0.0369, and lastly the factor of rotational speed at 0.048. For roundness, DOC is found as the most significant factor which is 0.0081, followed by the factor of rotational speed. Meanwhile, for eccentricity, the factor of feed rate and interaction between feed rate and rotational speed is found the most significant, which is 0.0349. While for dimension error, the most significant factor is the interaction between DOC and feed rate at 0.0021.

2. Optimization was done on combination parameter to optimize the error on water jet turning machine. The combination parameter is DOC= 0.1mm, feed rate= 3mm/min, rotational speed= 90rpm. The optimization resulting the best minimum value on responses which are surface roughness= 4.15321µm, roundness= 1.26137µm, eccentricity= 0.016524 µm and diameter error= 0.00340mm.

5.1.1 Sustainable design and development

AWJT is known as one of the types of water jet machining. The cutting tool in water jet machining usually used pressurized water, and this process can category as environmentally friendly due to the freshwater stream is used. This process can machine the most hardness metals and unique material with accuracy without producing heat and indirectly, noxious gases emitted. Using AWJT, there is no special treatment required to clean up after finishing this machining. The garnet sand used in this process can be quickly disposed of in the landfill.

5.1.2 Complexity

The complexity found while operating this machine is during the setup process. As you know, the AWJ machine at this university needs to be operated manually. Therefore, when ensuring the jig center only uses a ruler, DTI, and water level to ensure the jig's correct position. During the process, it takes a lot of time because it uses human ability and precision. The machine coordinates should be set manually, which required a large number of specimens to be used to get the required coordinates.

5.1.3 Life Long Learning (LLL)

Lifelong Learning (LLL) obtained after conducting this experiment is a new experience to operate the AWJT machine from the beginning process to the end that will apply one day when it has a career. In fact, undergoing this experiment adds to the quality of life to be more independent and learn to plan something carefully. One of the tools used is the Design of Experiment (DoE), which uses Design-Expert software to improve engineering skills in oneself. DoE is a crucial tool to start some experiments on a discovery. The majority of engineering industries use these tools to solve problems. Besides, learning about ANOVA also increased after this experiment.

5.2 Recommendation

Experimental results showed that the minimum value of surface roughness give a huge influence on the factor of DOC of 0.3 mm. But, it does not show the expected observation which is the small value of DOC (0.1 mm) should give a minimum value of surface roughness. This may due to the minimum number of the specimen is used during the experiment. So, a large number of specimens should be used for the next experiment about the surface roughness of the Inconel 718 alloy in order to identify the most significant factor, and further investigation should be conducted. The duration of the experiment is quite limited due to the Covid-19 that occurs and the use of the laboratory is very limited in fact it must follow the work schedule of the staff involved. Therefore, provide appropriate action such as extending the duration of the project is a good action. Furthermore, the validation error for this experiment is not conducted due to the machine used need to maintenance. Thus, further research needs to be done to make sure the validation error is below 10%.

REFERENCES

Nouhi, K. Kowsari, J.K. Spelt, M. Papini (2016). Abrasive jet machining of channels on highly-curved glass and PMMA surfaces. *Wear* 356-357(2016) 30-39.

Ushasta Aich, Simul Banerjee, Asish Bandyopadhyay, Probal Kumar Das (2014). Abrasive Water Jet Cutting of Borosilicate Glass. *Procedia Materials Science 6*, 775-   785.

Jain, V. K. (2002). Advanced Machining Process. *Allied Publishers Private Limited, India.*

Ravindra K. Palakudtewar and Sharad V. Gaikwad (2012). Dry Machining of Superalloy: Difficulties and Remedies. *International Jounal of Science and Research(IJSR).*

D.G Thakur, B. Ramamoorthy, L. Vijayaraghavan (2009). Study on the machinability characteristic of superalloy Inconel 718 during high speed turning. *Manuacturing Engineering Section, Mechanical Engineering Department, IIT-Madras, Chennai 660 036, Tamilnadu, India.*

K. N. Amato, S. M. Gaytan, L.E. Murr, E. Martinez, P.W. Shindo, J.Hernandez, S. Collins, F. Medina(2012). Microstructure and mechanical behavior of Inconel 718 fabricated by selection laser melting. *Acta Materialia 60*. 2229-2239.

94

Fuat Kartal, Zekeriya Yerlikaya, Hasan Gokkaya (2016). Effects of the machining parameters on surface roughness and macro surface characteristics when the machining of Al-6082 T6 alloy using AWJT. *Measurement 95* 216-222.

Vivek Bhandarkar, Virendra Singh, T.V.K. Gupta (2019). Experimental analysis and characteristization of abrasive water jet machining of Inconel 718. *Materials Today: Proceedings.*

Rajesh Patel K. and Dr. S. Srinivas(2017). Abrasive Water Jet Turning of Aluminum-silicon Carbide Metal Matrix Composites. Proceedings of 10th International Conference on Precision, Meso, Micro and Nano Engineering (COPEN10), Indian *Institute of Technology Madras, Chennai-600 036 INDIA.*

Eckart Uhlmann, Karsten Flogen, Michael Kretzschmar, Fabian Faltin (2012). Abrasive water jet turning of high performance materials. 5th CIRP Conference on High Performance Cutting. *Procedia CIRP 1* 409-413.

Tarek M. Ahmed, Ahmed S. El Mesalamy, Amro Youssef, Tawfik T. El Midany (2018). Improving surface roughness of abrasive waterjet cutting process by using statistical modelling. *CIRP Journal of Manufacturing Science and Technology* 22 30-36.

Dun Liu, Chuanzhan Huang, Jun Wang, Hongtao Zhu, Peng Yao, ZengWen Liu (2014). Modeling and optimization of operating parameters for abrasive waterjet turning alumina ceramics using response surface methodology combined with Box-Behnken design. *Ceramic International 40* 7899-7908.

95

Arola D and Ramulu M.(1997). Material removal in abrasive water jet machining of metals and a residual stress analysis. *Wear* 302-83.

Adnan Akkurt (2009). A surface properties of the cut face obtained by different cutting methods from AISI 304 stainless steel materials. *Indian Journal of Engineering & Materials Sciences.* Vol. 16, pp. 373-384.

M. Hashish(2016). Turning with abrasive water jets- A first investigation. *Journal of Engineering for Industry.* Vol. 109/287.

Hlavacek P, Crarach J., Hloch S., Vasilko K., Klichova D., Klich J.(2015). Sandstone turning by abrasive water jet. *Rock Mech Rock Eng.* 2489-93.

K. Balamurugan, M. Uthayakumar, S, Gowthaman, R. Pandurangan(2018). A study on the compressive residual stress due to water jet cavitation peening. *Engineering Failure Analysis 92*. 268-277.

Weiyi Li, Hongao Zhu, Jun Wang, Yasser M. Ali, Chuanzhen Huang (2013). An investigation into the radial mode abrasive water jet turning process on high tensile steels. *International Journal of Mechanical Sciences.* 365-376.

Sadasivam, A. Hizal, D. Arola(2009). Abrasive waterjet peening with elastic prestress: A parametric evaluation. *International Journal of Machine Tools and Manufacture.* 134-141.

Alberdi, A. Rivero, T. Artaza, A. Lamikiz(2017). Analysis of alloy 718 surfaces milled by abrasive waterjet and post-processed by plain waterjet technology. *Procedia Manufacturing 13.* 679-686.

Connelly and L.M. (2008). Pilot studies. *Medsurg Nursing.* 17(6). 411-2

Hertzog and M.A. (2008). Considerations in Determining Sample Size for Pilot Studies. *Research in Nursing and Health.* 180-191.

Mohammad Jafar Haddad, Fereshteh Alihoseini, Mostafa Hadi, Meysam Hadad, Alireza Fadaei, Aminollah Mohammadi (2009). An experiment investigation of cylindrical wire electrical discharge turning process. *International Journal Advanced Manufacturing Technology.* 46:1119-1132.

N. Satheesh Kumar, Ajay Shetty, Ashay Shetty, Ananth K., Harsha Shetty (2012). Effect of spindle speed and feed rate on surface roughness of Carbon Steels in CNC Turning. *Procedia Engineering.* 691-697.

Ashish Kumar Srivasta, Akash Nag, Amit Rai Dixit, Sandeep Tiwari, Jiri Scucka, Michel Zelenak, Sergej Hloch, Peter Hlavacek (2017). Surface integrity in tangential turning of hybrid MMC $A359/B_4C/Al_2O_3$ by abrasive waterjet. *Journal of Manufacturing Processes* 28. 11-20.

97

A C Arun Raj, S Senkathir, T Geethapriyan, J Abhijit (2018). Experimental investigation of abrasive waterjet machining of Nickel based superalloy (Inconel 625). *IOP Conference Series: Materials Science and Engineering. 402 012181.*

Dharmagna R. Tripathi, Krupang H. Vachhani, Soni Kumari, Dinbandhu, Kumar Abhishek (2020). Experimental investigation on material removal rate during abrasive water jet machininh of GFRP composites. *Material Today: Proceedings.*

Niranjan C.A, Srinivas S, Ramachandra M (2018). An experimental study on depth of cut of AZ91 magnesium alloy is abrasive water jet cutting. *Materials Today: Proceedings . 2884-2890.*

J. Wang (2008). A new model for ppredicting the depth of cut in abrasive water jet contouring of alumina ceramics. *Journal of Material Processing Technology 209.* 2314-2320

D.M D'Addona, Sunil J Raykar, M M Narke (2017). High speed machining of Inconel 718: tool wear and surface roughness analysis. *Procedia CIRP 62.* 269-274

M. El-Hofy, M. O. Helmy, G. Escobar-Palafox, K. Kerrigan, R. Scaife, H. El-Hofy (2018). Abrasive water jet machining of multidirection CFRP laminates. *Procedia CIRP 68.* 535-540.

Uma Maheshwera Reddy Paturi, Harish Devarasetti, Suresh Kumar Reddy Narala (2018). Application of regression and artificial neutral netwotk analysis in modelling of surface

roughness in hard turning of AISI 52100 steel. *Materials Today : Proceedings 5*. 4766-4777.

W. N. F. Mohamad, M. S. Kasim, M. Y. Norazlina, M. S. A. Hafiz, R. Izamshah, S. B. Mohamed. Effect of stand-off distance on the kerf characteristic during abrasive water jet machining. *Results in engineering 6*. 100101.

Popan, I. A., Contiu, G., Campbell, R. I. (2017). Investigate on stand-off distance influence on   kerf characteristics in abrasive water jet cutting of composite materials. *MATEC Web of Conference.*

Christy Atika Sari, Muhamad Wahyu Kuncoro, De Rosal Ignatius Mores Setiadi, and Eko Hari Rachmawanto. (2018). Roundness and Eccentricity Feature Extraction for Javanese Handwritten Character Recognition based on K-Nearest Neighbor. *2018 International Seminar on Researvh of Imformation Technology and Intelligent System (ISRITI).*

H. H. Tian, Y. X. Wang and H. X. Wang. (2020). Effect of Eccentricity on Roundness Measurement Accuracy for Cylindrical Components with Large Radius. *MAPAN-Journal of Metrology Society of India.*

APPENDICES A

Sample 1
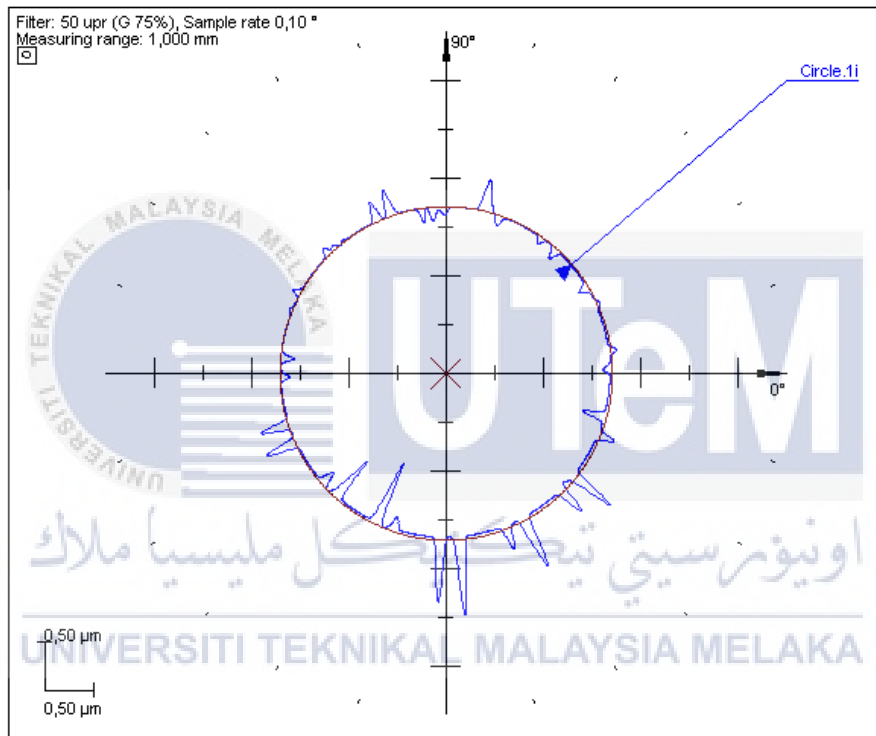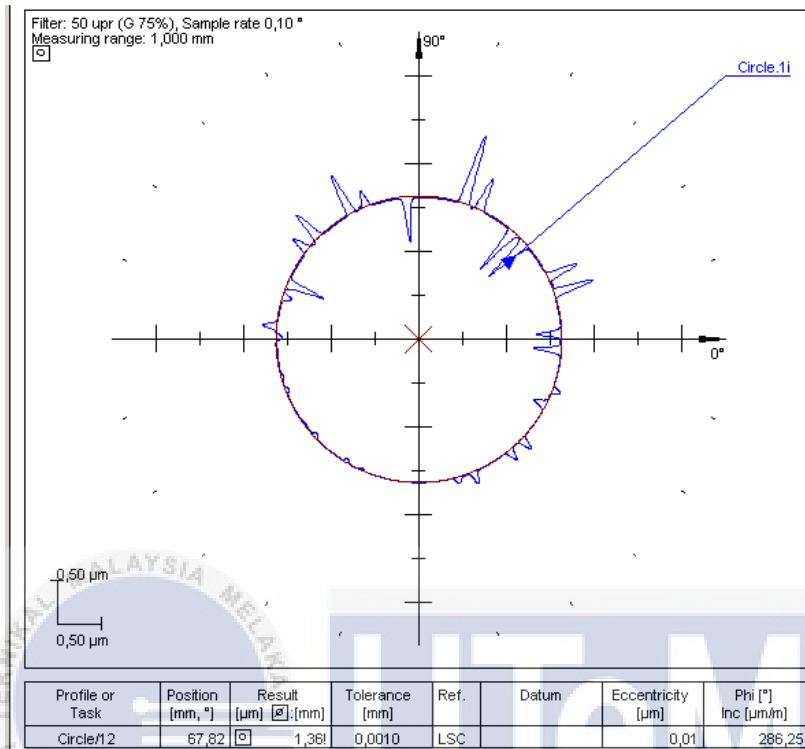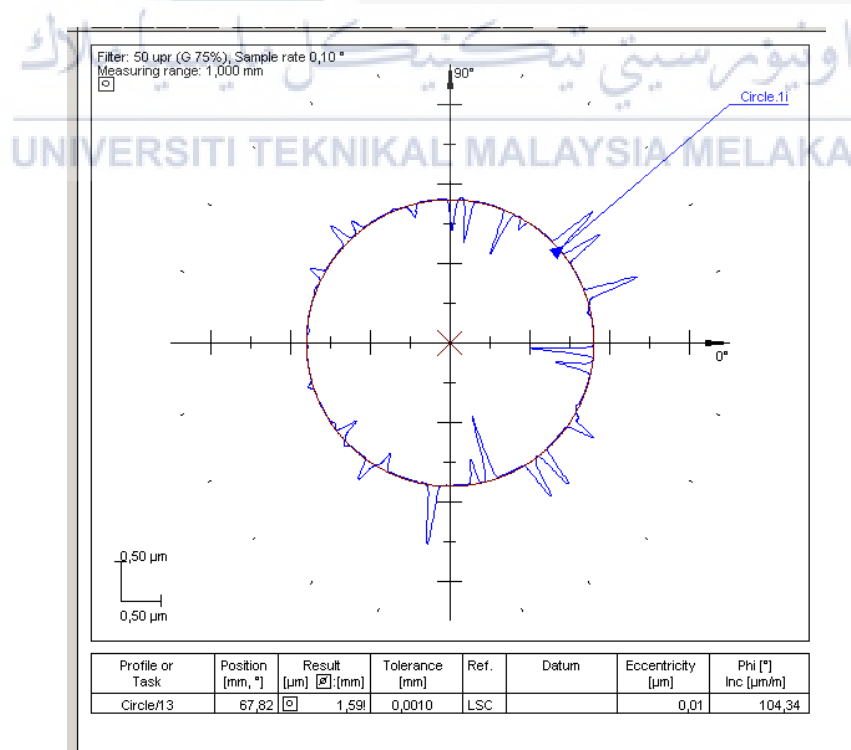

Profile or Task	Position [mm, °]	Result [µm] ⌀:[mm]		Tolerance [mm]	Ref.	Datum	Eccentricity [µm]	Phi [°] Inc [µm/m]
Circle/10	67,72	⊙	1,46!	0,0010	LSC		0,02	120,55

Sample 3

Profile or Task	Position [mm, °]	Result [µm] ⌀:[mm]		Tolerance [mm]	Ref.	Datum	Eccentricity [µm]	Phi [°] lnc [µm/m]
Circle/12	67,82	⌀	1,36!	0,0010	LSC		0,01	286,25

Sample 4

Profile or Task	Position [mm, °]	Result [µm] ⌀:[mm]		Tolerance [mm]	Ref.	Datum	Eccentricity [µm]	Phi [°] lnc [µm/m]
Circle/13	67,82	⌀	1,59!	0,0010	LSC		0,01	104,34

101

Sample 5

Filter: 50 upr (G 75%), Sample rate 0,10 °
Measuring range: 1,000 mm

Circle.1i

90°

0°

0,50 µm

0,50 µm

Profile or Task	Position [mm, °]	Result [µm] ⌀:[mm]	Tolerance [mm]	Ref.	Datum	Eccentricity [µm]	Phi [°] Inc [µm/m]
Circle/14	67,82	1,61!	0,0010	LSC		0,05	245,92

Sample 6

Filter: 50 upr (G 75%), Sample rate 0,10 °
Measuring range: 1,000 mm

Circle.1i

90°

0°

0,50 µm

0,50 µm

Profile or Task	Position [mm, °]	Result [µm] ⌀:[mm]	Tolerance [mm]	Ref.	Datum	Eccentricity [µm]	Phi [°] Inc [µm/m]
Circle/15	67,82	1,82!	0,0010	LSC		0,01	143,40

Sample 7

Profile or Task	Position [mm, °]	Result [µm] ⌀:[mm]	Tolerance [mm]	Ref.	Datum	Eccentricity [µm]	Phi [°] Inc [µm/m]
Circle/16	67,30	1,53!	0,0010	LSC		0,03	174,70

Sample 8
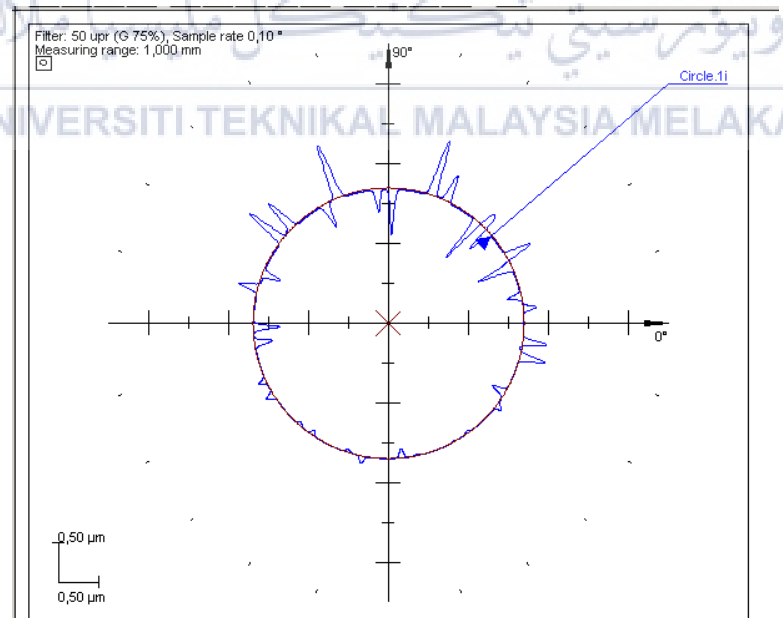
Profile or Task	Position [mm, °]	Result [µm] ⌀:[mm]	Tolerance [mm]	Ref.	Datum	Eccentricity [µm]	Phi [°] Inc [µm/m]
Circle/17	67,20	1,31!	0,0010	LSC		0,01	273,45